



POLITECNICO
MILANO 1863

SCHOOL OF INDUSTRIAL AND INFORMATION ENGINEERING
MASTER OF SCIENCE IN NUCLEAR ENGINEERING

Graphite Structure And Its Mechanical Properties

Supervisor: Prof. Marco BEGHI

Author:
Nermeen ELAMRAWY
ID. 894371

Academic Year 2018 - 2019

CONTENTS

Contents	2
Abstract	6
Summary.....	7
List of Figures	10
Chapter 1	11
Graphite Structure	11
1.1 Introduction	11
1.2 Carbon Material Properties	12
1.3 Crystal Lattice Of Graphite	13
1.4 Graphite Layer Packing	14
1.5 Formation Of Graphite	16
1.5.1 Types Of Graphite	17
Chapter 2	21
Defects In Graphite Lattice	19
2.1 Dislocations In Graphite	19
2.2 Boundary Structure In Graphite	24
2.3 Stacking Faults	24
2.4 Defects Of Carbon-atoms Bonding in Graphite layers	25
2.5 Lens Shaped Defects	26
2.6 Foreign atoms.....	26
2.7 Formation Energy Of Graphite Defects	30
2.7.1 Interstitials	32
2.7.2 Sheared Interstitials	34
2.7.3 Vacancies	37
2.7.4 Interstitial-Vacancy (I-V) Pair	39
2.7.5 Stone-Wales Defect	42

Chapter 3	43
Mechanical Properties Of Graphite	43
3.1 Density	44
3.2 The Mechanical Properties Of Single Crystal Graphite	44
3.3 The Elastic Constants Of Polycrystalline Graphite	52
3.4 The Theory Of Elastic Constants Of Polycrystalline Graphite	53
3.5 The Damping Properties Of Graphite	56
3.6 Creep In Graphite	58
3.7 Fracture Of Graphite	62
3.7.1 Highly Oriented Graphite	62
3.7.2 Polycrystalline Graphite	63
3.8 Yielding	65
3.8.1 Quasi-Static Strengths	65
3.9 Fatigue in Graphite	67
3.10 Friction in Graphite	69
4 Conclusion	71
5 References	72

Acknowledgement

Firstly Alhamdulillah and praise to Allah who gave me the guidance, and the opportunity and provide me the strength needed to accomplish this work, and ask for forgiveness for all the moments of despair.

Thanks Prof.Beghi for your understanding and instructions, it was my pleasure working with you.

My Family, Thanks SUPER Dad for helping me in achieving my ambition, brothers (Abd-El-Rahman and Muhammed) and Marwa thanks for always being there when needed.

Love, Thanks for your help and all the support all the way.

Mom, Wish you were with me, ALWAYS!

Abstract

Graphite is used in several applications starting from pencils to nuclear reactors, with other applications in between; such as lubricants, electrodes, batteries, solar panels and collimators. The properties of graphite were of extensive investigations for a few decades ago, and it was widely used in nuclear reactors. More recently, a new interest in graphite properties has been triggered by some specific applications. Namely, graphite or graphitic materials are adopted in accelerator technology to build beam collimators and beam dumps, as in LHC accelerators at CERN.

In this thesis, pre-irradiation graphite properties are discussed to understand the radiation effect on the crystals and find ways to prevent severe mutation if any. Here, we start with graphite crystal structure and the different types of graphite, then how lattice structure differentiates the defects propagation vacancies and interstitial, which in turn have an influence on the mechanical properties of the graphite which is discussed in the third chapter.

Sinossi

La grafite è utilizzata in diverse applicazioni che vanno dalle matite ai reattori nucleari, con altre applicazioni intermedie; come lubrificanti, elettrodi, batterie, pannelli solari e collimatori. Le proprietà della grafite sono state di ampie ricerche per alcuni decenni fa, ed è stato ampiamente utilizzato nei reattori nucleari. Più recentemente, un nuovo interesse per le proprietà della grafite è stato innescato da alcune applicazioni specifiche. Vale a dire, i materiali grafite o grafitici sono adottati nella tecnologia dell'acceleratore per costruire collimatori di fascio e discariche, come negli acceleratori LHC del CERN.

In questa tesi, le proprietà della grafite pre-irradiazione sono discusse per comprendere l'effetto delle radiazioni sui cristalli e trovare modi per prevenire la mutazione di severe, se presente. Qui, iniziamo con la struttura dei cristalli di grafite e con i diversi tipi di grafite, quindi come la struttura reticolare differenzia i vani di propagazione dei vuoti e gli interstiziali, che a loro volta influenzano le proprietà meccaniche della grafite che viene discussa nel terzo capitolo.

Summary

Graphite is a crystalline allotropic form of carbon atoms and in perfect lattice these carbon atoms are in parallel layers, graphite packing is of two types; hexagonal which is more stable and Rhombohedral. In hexagonal lattice the row of atoms in of the layers is above or under the centers of hexagonal in the neighboring layers hence the order of stacking is ABABA. On the other hand the rhombohedral (trigonal) lattice consists of the order of ABCABC. Artificial graphite is composed by both rhombohedral and hexagonal structure together in the crystal.

There are two types of highly disordered carbon layers which can be introduced; Non-graphitizing carbons do not yield the full three-dimensional order even when heated for long period up to 2000°C, Graphitizing carbon begin to show a reduction in their defects on heating up to about 1200°C and become quite well aligned at 2200°C. The changes in the process changes the characteristics of the graphite and hence we have several types of graphite; Natural Graphite, Kish graphite which crystallizes in the course of smelting iron, Flake graphite, Amorphous graphite, Vein graphite, Synthetic graphite which is usually formed by the progressive dehydrogenation and polymerization of hydrocarbon materials.

Graphite contains widespread dislocations, The rhombohedral formation is by heavy shear stacking is about ten layer planes after deformation and decreases with annealing till reaching zero when the annealing temperature is 3000°C. Partial dislocations also formed because of the vacancy or the interstitial loops causing a stacking fault due to irradiation damage loops of edge dislocation normally occur in graphite by removal or insertion of a circular or hexagonal area of base plane.

Twinning in graphite is corresponds to the insertion of one additional hexagon in other layer plane or generated by the alignment of the frequently observed basal dislocation to form a wall and the stresses of this wall can be relieved by slip which generates further dislocations and the band grows through the crystal.

Defects in atomic bonds in graphite layers. These includes, vacancies in the hexagonal network of a carbon layer (Schottky defects) and also displacement of carbon atoms from lattice point to interstitial positions (Frenkel defects). An accumulation of schottky defects may bring about a disruption of the carbon network leading to formation of the so-called "pliers" which cause the formation of screw dislocations and the other distortions of the carbon network. In the vicinity of such defects, the crystal lattice swells as a result of repulsion between the groups of atoms with broken bonds. Accumulation of vacancies leads to formation of voids in graphite crystals.

Foreign atoms enter between layers and also occupy the vacant sites in carbon layers these cause defects. This is used to lamellar graphite compounds as the atoms and molecules are able to enter in large numbers into the interlayer regions. As known interstitial impurity atoms has the role of electrons donors and acceptors also point defects and dislocations act as acceptors.

Graphite defects will affect its mechanical properties, the grain structure of the graphite affects heavily its mechanical properties, as known there is graphite with fine grains and some medium-grained depending on the method of manufacture as well as the precursor materials used during manufacturing. Graphite is considered as a brittle material which requires considerations of non-uniform stresses. There is a remarkable difference in the atomic binding, especially between the tight binding of atoms is the basal planes themselves due to the existence of the covalent bonds, these differences in the atomic binding affect the elastic, plastic and fracture behavior in mono-crystalline and polycrystalline graphite.

It was observed that the elastic modulus was always higher on cooling on the part of the curve where the modulus increased with temperature, also according to Bortz and Lund the maximum of the modulus decreased with increasing numbers of cycles. Andrew and Sato showed that the more graphitized the material the more the modulus in increased by temperature, these variations of modulus with temperature are based on the belief the crystals show normal dependence of elastic modulus on temperature.

Cyclic stressing produces hysteresis loops, the hysteresis increase with the degree of perfection in graphite, the observation of hysteresis loops in graphite crystals associated only with the basal shear mode have led many researchers to accompany the hysteresis of polycrystalline carbons and graphite with basal slip or cracking.

The behavior of commercial graphite like reactor graphite under tension stress is never linear when the stress is released permanent set is observed even after small stresses and then after several stresses hysteresis loops are formed. graphite remains in the elastic region while being in these loops cycling between the same stress limits producing superimposed loops. The apparent modulus decreases as the stress range in the cycling increases.

Polycrystalline graphite also shows less common modes of deformation, the creep at low temperature change conditions, a transient creep associated with the commonly observed permanent set and also a marked creep when the temperature approaches the highest heat treatment temperature.

Green and Zukas have observed that the tensile creep deformation is accompanied with numerous small cracks because of dislocation movement under tensile stress from the crack tip by climb, vacancies flowing from the dislocations to the crack tip or interstitial on the opposite direction, the cracks absorb the vacancies and the dislocations are emitted from the tips and that contributes to the strain.

The effect of adsorbed impurities on the frictional properties as in diamond the friction coefficient is about 0.5, when clean diamond surfaces are rubbed to each other. the surface became darker and as temperature is raised. Although this darkening happens below 1000°C, the film formed is stated to be identical with graphite in chemical and physical properties.

List of Figures

Fig. 1 Schematic representation of single graphite layer	13
Fig. 2 Hexagonal unit cell	14
Fig. 3 Rhombohedral graphite unit cell.....	15
Fig. 4 The production of Rhombohedral phase by boundary dissociation	20
Fig. 5 The Burgers vector.....	21
Fig. 6 Formation of extended nodes by fusion of dislocation ribbons	22
Fig. 7 Development of interstitial and vacancy loops	23
Fig. 8 (STM) topographic images of graphite defects.....	28
Fig. 9 (STM) topographic images	29
Fig.10 Adatoms	30
Fig. 11 Interstitial configurations in graphite.....	32
Fig. 12 Interstitial adatoms.....	34
Fig. 13 Sheared interstitial	36
Fig. 14 The simple Vacancies in graphite lattice	38
Fig. 15 Vacancies	39
Fig. 16 The intimate I-V pair in sheared graphite	40
Fig. 17 The recombination process between an interstitial and a vacancy in unsheared graphite.....	41
Fig. 18 Stone-Wales defect	42
Fig. 19 Variation of reciprocal Young's modulus with angle to hexagonal axis in a graphite crystal.....	48
Fig. 20 Variation of reciprocal rigidity modulus with angle to hexagonal axis in a graphite crystal.....	49
Fig. 21 comparison of data for graphite compressibility	51
Fig. 22 Stress strain curve of graphite	56
Fig. 23 tension in commercial graphite	57
Fig. 24 (a) High temperature creep	61
Fig. 24 (b) Normalised strain in normalized square root of time.....	62
Fig. 25 Illustration of crack structures in graphite crystals formed by glide.....	63
Fig. 26 Variation of coefficients A and B with heat-treatment temperature for petroleum coke graphite	64
Fig. 27 The endurance limit.....	68
Fig. 28 Typical specimen broken	69
Fig. 29 (a), (b) The relative movements of lamellae of graphite.....	70

Graphite Structure

1.1 Introduction

Graphite is a crystalline form of the element carbon and it is the most stable phase of carbon, graphite atoms are arranged in a hexagonal and rhombohedral structure discussed in details in this chapter. It occurs naturally in this form and is the most stable form of carbon under standard conditions. Under high pressures and temperatures it converts to diamond. Graphite is used in pencils and lubricants. Its high conductivity makes it useful in electronic products such as electrodes, batteries, and solar panels, also it is used in the nuclear reactors as a moderator because of its low neutron absorption cross section and also as a refractory material.

Carbon fiber-reinforced graphite (CFC) is used a collimation material, CFC consists of a graphite matrix filled with carbon fiber, this cause the material to be reinforced due to their high strength and also enhance the thermal and electrical conductivity.^{[16],[17]} Molybdenum carbide- graphite (MoGr), is used as a collimator material for HL-LHC, as it has a characteristics of high thermal conductivity and low thermal expansion which hold high thermal load.^{[16],[18]} As Molybdenum itself has good high melting point, low thermal expansion coefficient (thermal properties), it also has high mechanical strength and electrical conductivity, with its low average atomic number ($Z \sim 6.5$), as a specific formulation is adopted to maintain the percentage of Mo very small; otherwise the average Z would be much higher. Combine these Molybdenum properties with the low density and excellent thermal conductivity of Graphite, if we obtained a good graphitization we reach excellent thermal conductivity and low thermal expansion coefficient which make MoGr the ideal for primary and secondary collimators.^[14]

In this chapter we will discuss; natural and artificial graphite their crystals packing and carbon atom order in the ideal case and dislocation effects in the graphite lattice and Graphite in Nature, natural graphite is extracted from quarries, in different forms, which depend on the characteristics of the reservoir. The forms of graphite present in nature differ in morphology.

The following map illustrates the location of the largest natural graphite deposits in the world, and the production of the main producing countries.



Location of the main natural graphite deposits

1.2 Carbon material properties

Graphite is a crystalline allotropic form of carbon this gives graphite certain properties matching with carbon material properties such as low specific gravity, chemical inertness preserved up to 900k. However, for oxygen as it has been testified that graphite reacts with oxygen above this temperature, but doesn't get degraded. Proceeding with the properties, graphite also has high antifrictional power, large neutron attenuation factor with a low neutron absorption cross section, that's why graphite is used as a moderator in nuclear reactors and sublimation temperature above 3900k. Carbon materials can retain its mechanical properties at an sometimes above 3500k, the material resistivity change widely according to the heat treatment or material interaction with different substance. [1]

Artificial graphite has almost the same crystal structure of natural monocrystalline graphite, in pyrocarbon materials the distance between carbon layers is greater than the natural graphite. [1]

1.3 Crystal lattice of graphite.^[1]

In perfect lattice carbon atoms are almost in parallel layers, in room temperature the distant between two layers is $3.3538A^0$ where carbon atoms are distant from each other by $1.415A^0$ forming a hexagonal shape. The weak bonding between layers causing the difference between in-plane and out-of-plane characteristics, i.e. anisotropy which in short is difference in graphite characteristics. The layer of graphite is of two dimensions in order to isolate a unit cell we divide the layer into rhombus by parallel lines as shown in **figure 1**.

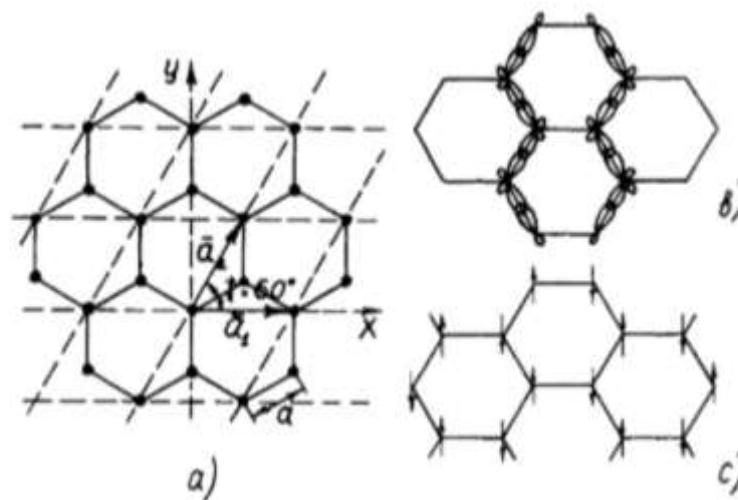


Figure (1) Schematic representation of single graphite layer

(a) primitive translation a_1 and a_2 and a unit cell of the single layer, (b) overlap of the wave functions in the formation of σ bonds, (c) π electrons spin distribution in the graphite layer.

There are two carbon atom per lattice cell and if we considered the layer area is S , the number of atoms in the layer, N , is given by

$$N = 2 \frac{S}{S_0} = \frac{4S}{\sqrt{3}a_0^2} \quad (1.1)$$

Where the area of the elementary rhomb

$$S_0 = (a_1 \cdot a_2) = \frac{1}{2} \sqrt{3} a_0^2 \quad (1.2)$$

where (a_1, a_2) are two translation vector correspond to a unit cell $|a_1| = |a_2| = a_0 = \sqrt{3}a \sim 2.46A^0$

The corner carbon atoms of the hexagonal shape are determined by the equivalence of the three bonds of the carbon atom with its three nearest neighbors in the layer, Carbon atoms are linked by two types of bonds:

1. Direct σ bonds

Sigma bonds are the strongest type of covalent bonds due to the direct overlap of orbital (head to head overlap), and the electrons in these bonds are referred to as σ -electrons, and take place in the sp^2 hybridization.^[2],figure1.b.^[1]

2. π bonds

Pi bonds are formed by the unhybridized Pi-electrons and in order to form this bonds the neighboring atoms spin should be antiparallel **figure1.c**. Due to π -electrons an additional bond is formed and strengthens the bond, but its still weaker than the sigma bond and due to this bond three dimensional graphite have its semi metallic properties and its metallic lustre .

1.4 Graphite Layer Packing.^[1]

There are two types; hexagonal unit cell and Rhombohedral graphite unit cell and as will be shown in the following, these two types are different in packing through the graphite layer, the structure of each layer is the same.

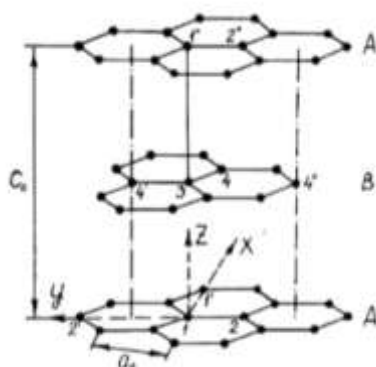


Figure 2

hexagonal unit cell

A,B indicate non-equivalent graphite layers

The hexagonal lattice unit cell was proposed by Bernal (1942) and named after him, it consists of a stack of parallel hexagonal net, the closest neighboring atomic spacing is $1.42 \times 10^{-8} \text{ cm}$ and the spacing between net planes is $3.35 \times 10^{-8} \text{ cm}$, the planes consists of four carbon atoms (1,2,3,4) shown in **figure 2**, while atoms (1, 1', 1'', etc) are on the same sub-lattice.

In hexagonal lattice the row of atoms in of the layers is above or under the centers of hexagonal in the neighboring layers as shown in **figure 2**. The order of stacking is ABABA, the period of recurrence of one type being equal to the double distance between two neighboring layers .

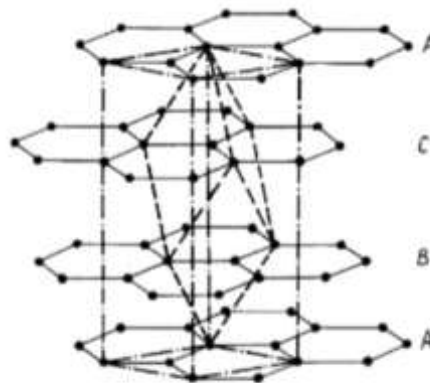


Figure 3

Rhombohedral graphite unit cell

The rhombohedron is defined by the dashed lines

A,B,C indicate non-equivalent graphite layers

The rhombohedral (trigonal) lattice consists of the order of ABCABC according to Boehm and Hofman, and this lattice was first proposed by Finch and Wilman who X-rayed an number of specimens of both natural and synthetic graphite and observed diffraction lines as shown in **figure3** could not be explained by hexagonal structure. The trigonal fraction in natural graphite is about 20% and decreased by heat treatment , this indicates that the hexagonal structure is more stable.

The graphite is freshly crystallized from molten iron 'kish' which consists of iron and silicon, forming an interlayer spacing of $3.3528 \pm 0.0002 \text{ \AA}$ when the graphite is treated by concentrated HCL, the iron is removed and the spacing expands and forms Ceylon

graphite. Ceylon, Bavaria, Korea and Travancore can be found in hexagonal or rhombohedral packing. Pyrolytic graphite is found in rhombohedral packing structure.^[13]

Treatment with hot strong acids also tends to rearrange successive layers in such a way that extensive sequence of a b c are suppressed, this treatment does not cause loss in carbon atoms yet the carbon atom networks become mobile in the strong acid and slip into new positions. By the contrast of strong acid effect, anodic bromine treatment increases the proportion of rhombohedral packing in the carbon recovered. Slip of networks also appears to occur when there is a mixture of rhombohedral and hexagonal regions in the graphite, this graphite is first converted to the ferric chloride crystal compound and then $FeCl_3$ is then expelled by heating. This treatment shows exclusively the hexagonal structure.

Artificial graphite is composed by both rhombohedral and hexagonal structure together in the crystal, according to Lipson and Stock, The ideal well crystallised artificial graphite is consisted of 17% rhombohedral graphite, in other case it has also been found that in artificial graphite sample of random orientation the hexagonal structure was absent and it is increased only a few percent (around 5%) by mechanical deformation such as grinding powdering.^[3] When heating to 2000 - 3000°C any rhombohedral packing is transformed into hexagonal and that indicates that the hexagonal packing is more stable.^[13]

Several investigations on natural graphite has indicated that they contain as much as 30% of rhombohedral material, unlike artificial graphite, mechanical deformation of natural graphite increase the proportion of rhombohedral crystal packing.

1.5 Formation of graphite

There are two types of highly disordered carbon layers which can be introduced; Non-graphitizing carbons do not yield the full three-dimensional order even when heated for long period up to 2000°C, Graphitizing carbon begin to show a reduction in their defects on heating up to about 1200°C and become quite well aligned at 2200°C. The formation of graphite is considered from initially pure hydrocarbon in the absence of oxidation, when the hydrocarbon is heated above 400°C, polymerization begins where the substance turn to be darker, condensed ring structures is formed if the hydrocarbon is initially of an aliphatic character; the relative ease of incipient polymerization depends on the molecular structure of the starting material. When the temperatures are above 1600°C another structural changes when exceeding the maximum temperature the graphite lines are observed to

increase in intensity and in sharpness, from 1600°C to 2800°C progressive graphitization occurs an increasing degree of three dimensional order is reached in the carbon polymer. These changes in the process changes the characteristics of the graphite and hence we have several types of graphite.

1.5.1 Types of Graphite

Near-ideal graphite is of three main types:

- (a) Natural Graphite
- (b) Kish graphite which crystallizes in the course of smelting iron.
- (c) Flake graphite
- (d) Amorphous graphite
- (e) Vein graphite
- (f) Synthetic graphite which is usually formed by the progressive dehydrogenation and polymerization of hydrocarbon materials.

Natural graphite

The carbon crystals in natural graphite shows variable perfection of ordering, it is obtained in the form of small flakes with a metallic luster. After removal of the grosser impurities and to get the highest purities it is refluxed with concentrated hydrochloric acid and washed with concentrated hydrofluoric acid.

Kish graphite

It is always similar in appearance to flaky natural graphite, the X-ray structure of kish and temper graphite is identical to natural graphite. However, lamellar, temper and nodular graphites are not perfectly crystalline as kish. At lower temperatures a proportion of the carbon may be present in polyatomic form or as hexagon rings.

Crystalline Flake

Flake graphite occurs as isolated, flat, plate like particles with either hexagonal if unbroken and when broken the edges can be angular edges. It is found in metamorphic rocks such as limestone, gneiss and schist and is distributed uniformly throughout the body of the ore or in concentrated, lens-shaped pockets. Natural flake has the widest range of use and accounts for about 49% of natural graphite consumption.

Amorphous graphite

It is formed by the metamorphism of previously existing anthracite coal seams. The term “amorphous” refers to its very small crystal size of particles, which are not visible unless viewed under magnification and its carbon content depends on that of its parent material. However, unlike coal, amorphous graphite is not used as fuel as it is difficult to ignite..

Vein graphite

Vein graphite or lump graphite, is believed to have hydrothermal origins and occurs in fissures or fractures, appearing as massive platy intergrowths of fibrous or crystalline aggregates. It is considered the rarest, most valuable, and highest quality form of natural graphite. It is formed from the direct deposition of solid, graphitic carbon from subterranean, high temperature fluids. Vein graphite has higher thermal and electrical conductivity, and it also has the highest degree of cohesive integrity of all natural graphite.

Synthetic Graphite

Highly ordered pyrolytic graphite or highly oriented pyrolytic graphite (HOPG) refers to graphite with an angular spread between the graphite sheets of less than 1° . This highest-quality synthetic form is used in scientific research, in particular, as a standard for scanner calibration of scanning probe microscopes. The name "graphite fiber" is also sometimes used to refer to carbon fiber or carbon fiber-reinforced polymer. There is also Bulk synthetic graphite which is formed by heating organic cokes to a high temperature in the absence of air; anthracites is heated in an electric furnace or coke particles are heated with pitch.

Defects in Graphite lattice

In this chapter we will discuss the defects in the graphite lattice due to thermal and chemical changes, the type of defects and the formation energy of such defects through different experiments and papers introduced earlier.

As we discussed the ideal structure of graphite lattice in the previous chapter and reached a conclusion of different material composition of graphite used in several chemical and industrial applications, these varieties comes from the fact that the real graphite differ from the ideal structure by the presence of lots of several defects occurs due to stacking faults, foreign atoms, bombarding graphite with ions or changing the thermal and chemical medium.

2.1 Dislocations In Graphite

Graphite contains widespread dislocations, the stacking fault enclosed by regions in the rhombohedral sequence and split into a separation $1000 - 2000A^0$. The deformation of the graphite and the production of the rhombohedral phase is by compression parallel to the hexagonal axis and the polycrystalline graphite is deformed by filing.

The rhombohedral formation is by heavy shear stacking is about ten layer planes after deformation and decreases with annealing till reaching zero when the annealing temperature is 3000^0C . However, due to the widely spread partial dislocations a region with rhombohederal stacking through four layers, leads to dislocations. The total dislocation in the basal plane split into partial of separation $1000 - 2000A^0$ with density explained as half of the area will be a stacking fault and the order is sequenced along c-axis. When shear stress in the same direction of dislocation line this will tend to force such dislocations apart producing forces of opposite sign on the screw components.

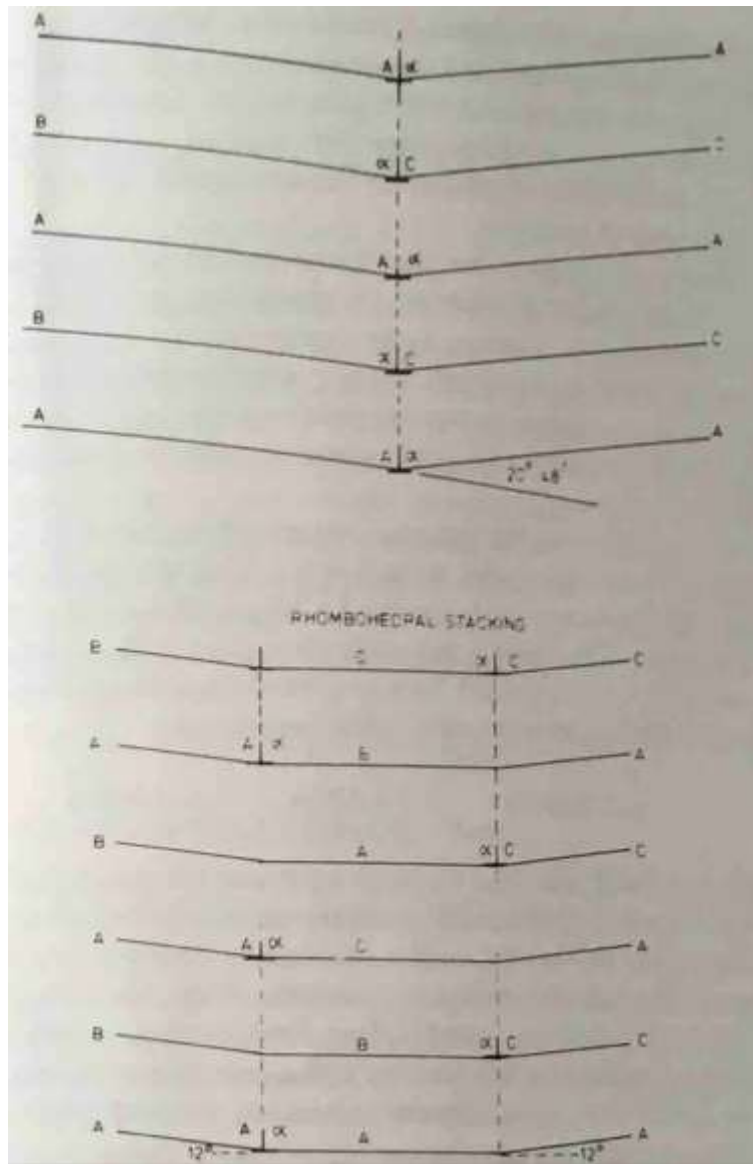


Figure 4

Figure 4 shows the production of rhombohedral phase by boundary dissociation. (a) Twin matrix boundary for $20^{\circ} 48'$ (b) dissociation of (a) with Burger's vectors αC and $A\alpha$ moving in opposite directions.

A different explanation of rhombohedral lines that it was superstructure reflection from an orthorhombic unit cell due to a small distortion of the hexagonal unit of the layer planes.

Let's introduce the term Burger's vector.^[4]

When calculating the Burgers vector practically, one may draw a rectangular clockwise circuit from a starting point to enclose the dislocation **Figure 5** The Burgers vector will be the vector from the START to the END of the circuit.

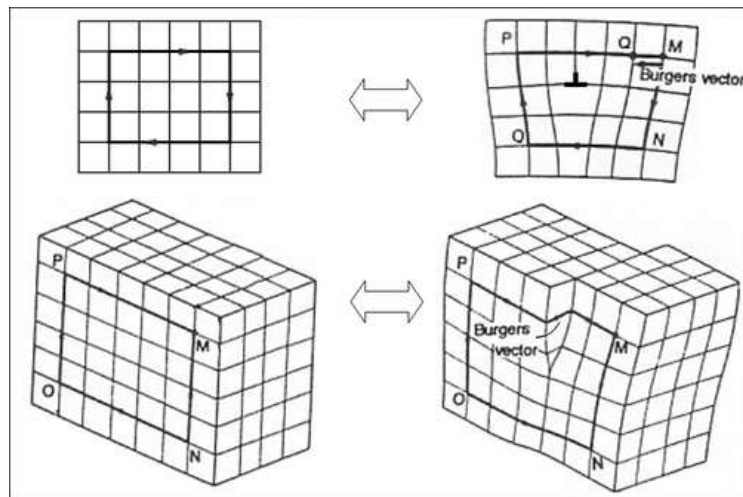


Figure 5

There are four possibilities for dislocations in graphite lattice.^[3]

1. Burger's vector and dislocation line in the basal plane.
2. Burger's vector perpendicular to the basal plane, dislocation line in the basal plane.
3. Burger's vector and dislocation line in non-basal directions.
4. Burger's vector in the basal plane, dislocation line parallel to hexagonal axis.

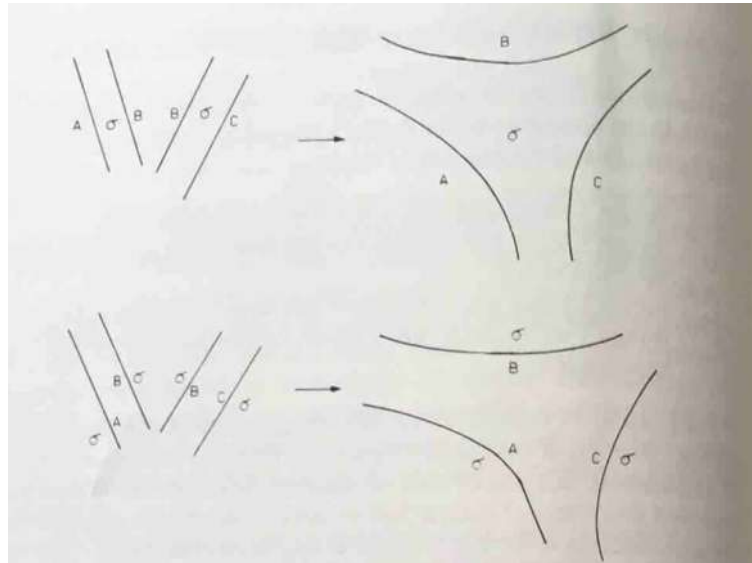


Figure 6

formation of extended nodes by fusion of dislocation ribbons. The basal plane contains six perfect lattice vectors denoted by AB, AC and BC and their negatives. The partial dislocations have Burger's vectors corresponding to the nearest neighbor positions denoted by $A\sigma, B\sigma$ and $C\sigma$ so the dislocation is $AB \rightarrow A\sigma + \sigma B$.

The dislocation form extended and contracted nodes shown in figure 6 and they are easy to observe because the separation between the partials varies from $500 \times 10^{-8} \text{ cm}$ to $1000 \times 10^{-8} \text{ cm}$. The partial dislocations repel each other but the stacking fault between them have opposing force.

Due to irradiation damage loops of edge dislocation normally occur in graphite by removal or insertion of a circular or hexagonal area of base plane, so the vacancy or the interstitial loops enclose a stacking fault and also cause partial dislocations. Figure 7 shows the interstitial loop consists of insertion of a new layer plane in c-staking in ABCAB, but if the loop becomes sufficiently large its energy can be reduced by nucleation of shear. The interstitial loops are not expected to shear because of the high barrier to spread of the lower energy stacking fault which is discussed later in this chapter.

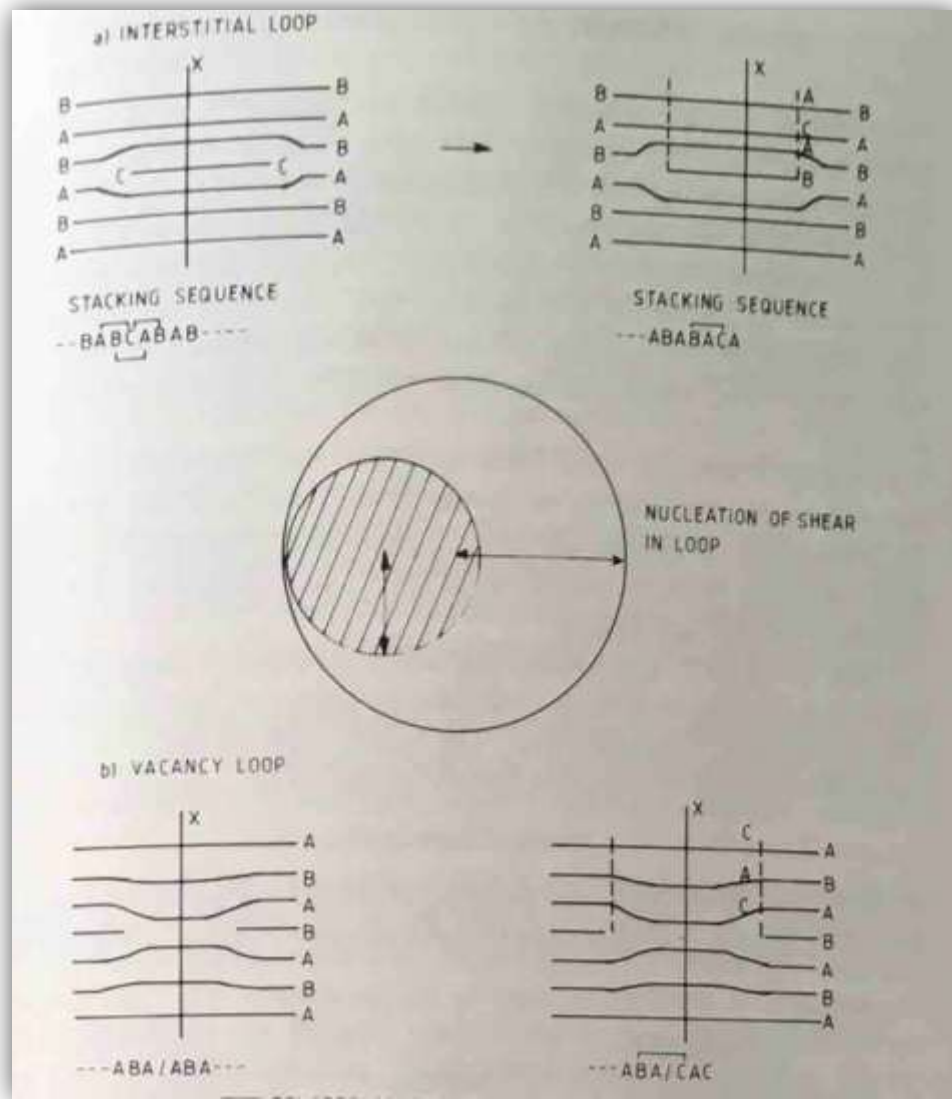


Figure7 Development of interstitial and vacancy loops

It is necessary for the lattice to collapse to form the loop of dislocation with minimum radius equals to $110 \times 10^{-8} \text{ cm}$. The stacking fault corresponds to A over A stacking.

2.2 Boundary Structure In Graphite.^[3]

Introducing twinning Crystal

Twinning occurs when two separate crystals share some of the same crystal lattice points in a symmetrical manner.^[5]

Twinning in graphite corresponds to the insertion of one additional hexagon in other layer plane or generated by the alignment of the frequently observed basal dislocation to form a wall and the stresses of this wall can be relieved by slip which generates further dislocations and the band grows through the crystal.

Non basal dislocations already described lead to macroscopic structural features whose studies are carried out by using optical microscopy with ingenious use of catalyzed etching techniques and experiments indicated the density of non-basal dislocations to be 10^3 to 10^5 cm^{-2} .

Some studies showed a screw dislocations with line parallel to hexagonal axis with large magnitude of burger's vector in the range of 150×10^{-8} to $1000 \times 10^{-8} \text{ cm}$. These observations include carbon blacks, Pyrolytic graphite and Ticondergo flake these materials are man-made can not be found in nature and are produced using thermal decomposition or using hydrocarbons like in *carbon black*^[11] due to producing defects in the graphite structure, which is discussed in details in the this chapter.

Carbon black is produced by thermal decomposition such as oil or natural gas as raw material called partial combustion method.

2.3 Stacking faults.^[1]

The most common defect occurs due to the alternation of layers and breaking the periodicity of the crystal structure, when the crystal is strained, and that's typically what happens in the turbostratum material are produced from the decomposition of the aromatic hydrocarbons " *is a hydrocarbon with sigma bonds and delocalized pi electrons between carbon atoms forming a circle.*"^[6] and then the products are being precipitated onto a heated substrate. Turbostratum in which the parallel layers shows no ordered stacking sequence, referred to carbons which have not heated to a sufficiently high temperature for ordering.

The average distance between the graphite layers, d , is a quantitative characteristic. For the degree of disorder, Bacon (1951) established a parameter to represent the fraction of graphite layers in the turbostratum state, p , when $p = 0$ corresponds to a perfect lattice and $p = 1$ represent a totally disordered lattice, these empirical quantities are related to the following expression ;

$$\tilde{d} = 3.440 - 0.086(1 - p) - 0.064(p - 1)p(\text{Å}) \quad (2.1)$$

So turbostratum material has average spacing; $\tilde{d} = 3.440 \text{ Å}$. Artificial graphite has intermediate structure as $\tilde{d} = 3.36 \text{ Å}$ so $p = 0.17$. according to Blackman (1960) so stacking faults are always present in graphite used in nuclear reactors.

Defect in the graphite is expected at high temperature and thermal equilibrium with high concentration such as vacancies, interstitial and Frenkel pairs which are discussed in details later in this chapter.

2.4 Defects of carbon-atoms bonding in Graphite layers

Defects in atomic bonds in graphite layers. These includes, vacancies in the hexagonal network of a carbon layer (Schottky defects) and also displacement of carbon atoms from lattice point to interstitial positions (Frenkel defects). An accumulation of schottky defects may bring about a disruption of the carbon network leading to formation of the so-called "pliers" which cause the formation of screw dislocations and the other distortions of the carbon network. In the vicinity of such defects, the crystal lattice swells as a result of repulsion between the groups of atoms with broken bonds. Accumulation of vacancies leads to formation of voids in graphite crystals.

2.5 Lens shaped defects

Discovered by Bonfiglioli and Mojoni (1964) with cross-sections ranging from 200 to 3000 Å and the thickness considered as several lattice parameters of natural graphite, this shape is formed due to the accumulation of vacancies and gives rise to edge dislocations and dislocation loops. Experiments by Henning (1965) showed the vacancies and dislocation loops increase in the graphite crystal when heated to high temperature between 1900 and 3400K, before that, in 1960 Rasor and McClelland estimated that vacancy formation energy in graphite to be as (7.7 ± 0.5) eV, near to the sublimation heat (7.4 eV).

Frenkel pairs arise when atoms are moved to interstitial sites and interstitials are placed between layers in the graphite lattice causing layers bending and sometimes lead to parting of layers. These defects are common if the graphite is irradiated with neutrons.

2.6 Foreign atoms

Foreign atoms enter between layers and also occupy the vacant sites in carbon layers these cause defects. This is used to lamellar graphite compounds as the atoms and molecules are able to enter in large numbers into the interlayer regions. As known interstitial impurity atoms has the role of electrons donors and acceptors also point defects and dislocations act as acceptors.

In order to obtain the perfect structural lattice under heat treatment, artificial carbon materials are divided into graphitizable which begin to change their structure at 1600 - 1800°C as their initial interlayer spacing is $\tilde{d} = 3.44\text{Å}$ and nongraphitizable not change their structure under heat treatment even at 2000°C as the interlayer spacing $\tilde{d} = 3.70\text{Å}$

The method of creating carbon materials is different, as the analysis of carbon particles from refined graphite, pyro graphite which is a man-made is not found in nature and is similar to graphite, but with some covalent bonding between its graphene sheets as a result of imperfections in its production.^[7] There is also kish-graphite which indicates that all these particles have a similar chemical composition, the fraction of impurities constituting several hundredths of a percent . All this material mentioned have a basic unit of a single graphite layer having one or another degree of imperfection. It should be known that a simple change in the parameters like the temperature or the size of the chamber used to produce pyrocarbons may alter the structure and in turn change the mechanical behavior of carbon materials.

At present, There are a lot of parameter affecting carbon structure:

- (a) The average distance between layers, \tilde{d} , which vary from 3.400 to 3.354Å;
- (b) The graphitization parameter, γ , gives the measure of the measure of three-dimensional order:

$$\gamma = \frac{3.400 - \tilde{d}}{0.086} \quad (2.2)$$

where 3.354Å is distance between layers in the least ordered structure graphite and to 0.086 Å is the difference between the values for the interlayer distances in the least ordered structure and in mono-crystalline graphite;

- (c) the average statistical size of the regions of coherent scattering in the basal plane (L_a) and in the perpendicular plane (L_c) determined from the broadening of X-ray lines:

$$L_{a,c} = \frac{K\lambda}{\beta \cos \theta} \quad (2.3)$$

Where λ is the wavelength and θ is the angle of X-ray, K is the factor of X-ray lines, β is the line's half-width.

- (d) the concentration of layer stacking faults.
- (e) the degree of preferred orientation of crystallites, $n(\varphi)$, which is determined from the relative intensity of X-ray lines $n(\varphi)/I(0)$

φ being the angle between the normal to the suitable plane and the preferred directions. When graphitizable materials are heat treated, the perfection of their crystal lattice increases, which manifests itself in a decrease of the value of the parameter \tilde{d} and an increases in the values of γ , L_a , L_c and $n(\varphi)$.

Modern imaging techniques reported by J. R. Hahn and H. Kang In 1999 allow a significant direct insight into the structure of defects by using different ions with certain energies discussed in the following ;^[8]

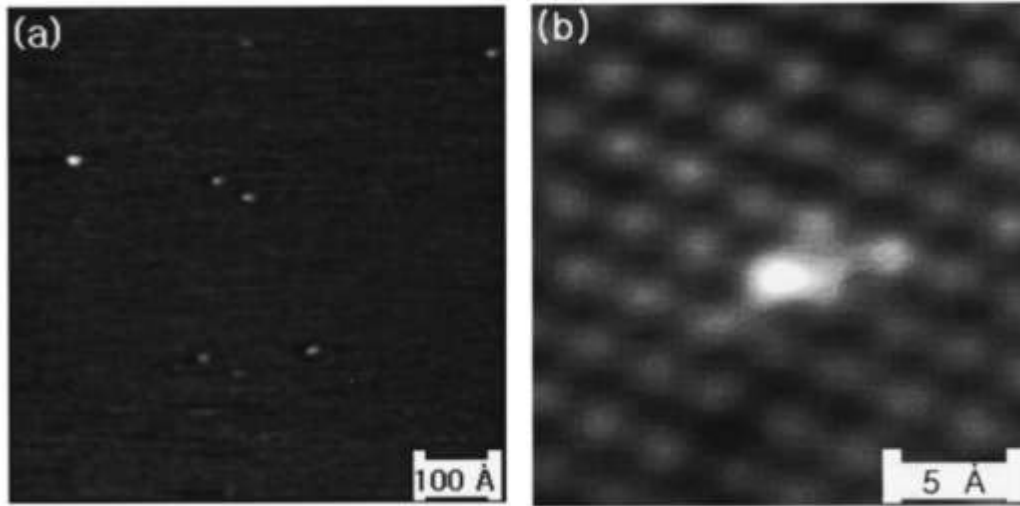


Figure (8)

(a) a large-scale image, Ion impact energy is 100 eV. Scan conditions are sample bias of 2100 mV and tunneling current of 0.5 nA.

(b) a high resolution image, ion impact energy is 60 eV, sample bias of 260 mV and tunneling current 03 nA.

Defect (carbon vacancies) and interstitial (noble gas) creation at graphite surfaces by bombarding energetic ions of Ar^{+1} and Kr^{+1} ions in the range of 40–100 eV causes hillocks of few nm in diameter or larger

Scanning tunneling microscopy (STM) topographic images of the defects created at a graphite surface by Ar^{+1} ion impact. A VD appears as a protrusion in STM image and so does an ID, but they can be distinguished from each other in the measurements of local tunneling barrier height.

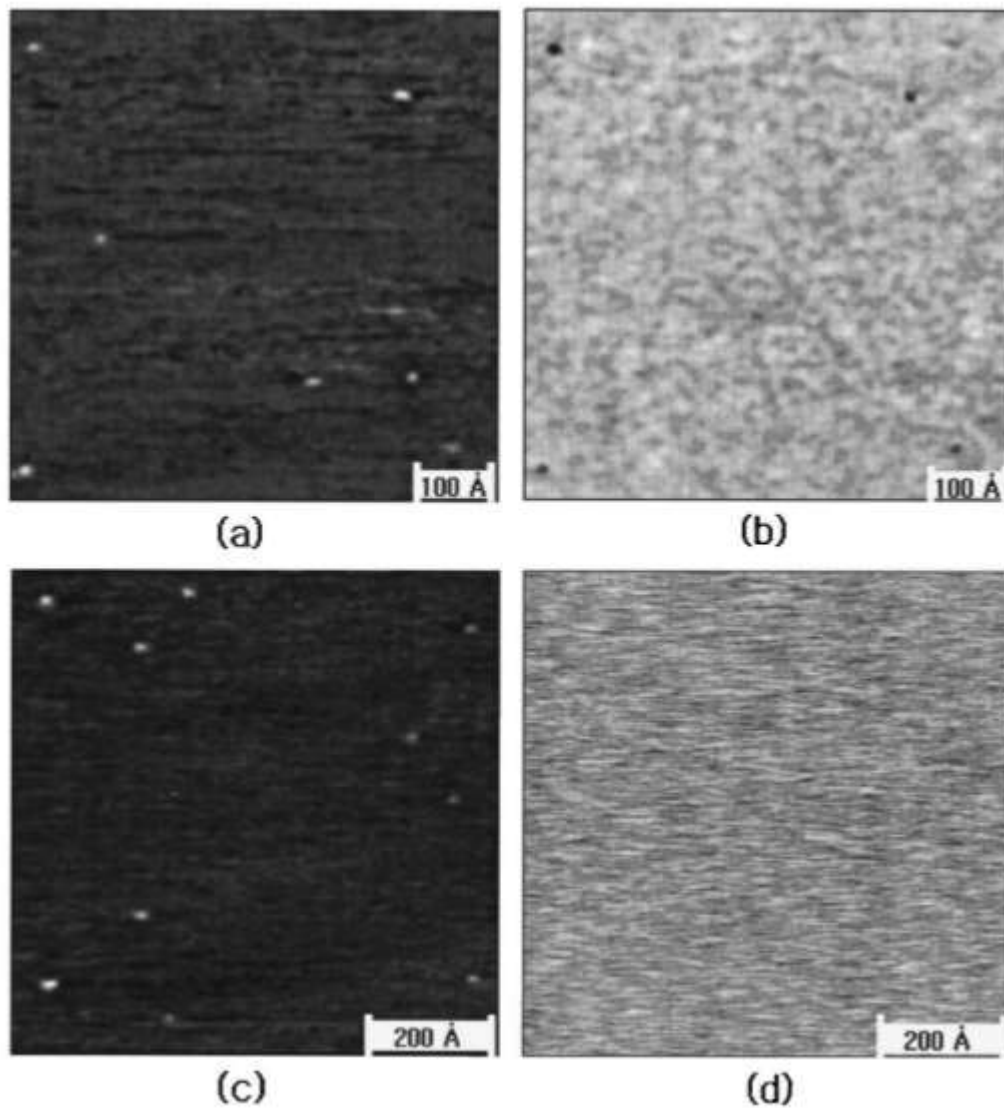


Figure (9)

- (a) STM topographic image of a graphite surface impacted with Kr^{+1} ions at 100 eV.
- (b) The image of tunneling barrier height obtained from the same region simultaneously with (a).
- (c) STM topographic image obtained after 50 eV Kr^{+1} impact.
- (d) The corresponding image of local barrier height from region (c).

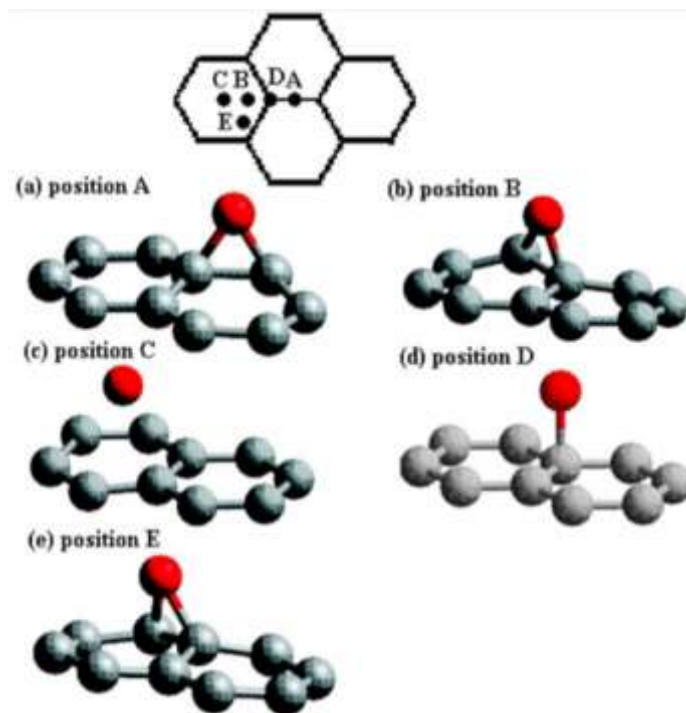
2.7 Formation Energy of graphite defects

In 2004 L. Li, S. Reich and J. Robertson have performed a computational method to calculate the formation energy of defects in the graphite, this paper showed the possible defects created in graphite which is as the following;

First let's introduce adatom term definition

"An adatom is an atom that lies on a crystal surface, and can be thought of as the opposite of a surface vacancy"^[9]

There are five high-symmetry positions of adatom on one single layer of graphite, shown in Fig. (10) The most important are A, the bridge site above the bond center between two layer atoms, C above the center of a hexagon of bonds, and D directly on top of an atom.



Figure(10) Light gray atoms are part of graphene, the adatom is dark red.

The formation energies E_f were obtained from the total energies of the supercells with a defect

$$E_f = E_d - E_{bulk} - n\mu \quad (2.4)$$

Where;

E_d is the total energy of the defected supercell;

E_{bulk} is the total energy of perfect graphite, which we calculated for supercells of the same size as used in the runs with the defects;

μ is the chemical potential of carbon, which we took as the total energy of graphite;

n gives the number of carbon atoms that were added, n , positive or removed, n , negative

After computations it was noticed that the lowest energy site is found to be the bridge site A the adatom is bonded to two layer atoms with a bond length of 1.51 Å, as seen in figure(10)a.

Meanwhile, the bond between the atoms within the layer weakens a little, increasing its length from 1.41 Å to 1.56 Å. Thus, the adatom is forming two reasonably strong bonds.

The next most stable position is E. This extra atom is similar to site A, except that the bond is tilted which allows the adatom to bond to two atoms with one slightly shorter bond of 1.5Å and one bond of 1.51 Å figure(10) (e) . The actual in-plane bond lengthens to 1.55 Å. The next most stable site is B figure(10) (c). where the adatom makes a shorter bond of 1.49 Å and a longer bond of 1.65 Å, which makes the in-plane bond to 1.52 Å. At the on-top site D the adatom bonds directly to only one layer atom in case we do not relax the atomic coordinates. We show this configuration in figure(10) (d); the bond length is 1.55 Å. This position is 1 eV less stable than site A. The symmetric on-top position D is unstable; relaxing the atomic positions allows the adatom to strain the graphene layer, so that it can form a shorter bond of 1.48Å to the nearest atom and a long bond of 1.7 Å to a second neighbor atom.

After relaxing the atoms in the graphene layer, the formation energy decreases by 0.5 eV to 7.2 eV; Finally, in position C above the center of a hexagon, the adatom does not make bonds to layer atoms, and this is the most unstable position with a formation energy of more than 8 eV. The adatom lies 1.66 Å above the graphite plane, at 2.15 Å from the atoms figure(11) (c). The formation energies of an adatom thus depends on the number of bonds the adatoms form with the carbon atoms in the layer. The formation energies are smallest 6.7 eV for adatoms that have two bonds to the graphene layer sites A, B, and E. Site D has two bonds with different lengths in the relaxed structure. Moreover, an adatom at D strongly strains the graphene sheet and makes the configuration less stable. Site C has the largest formation energy, because no bond forms between the adatom and grapheme.

2.7.1 Interstitials

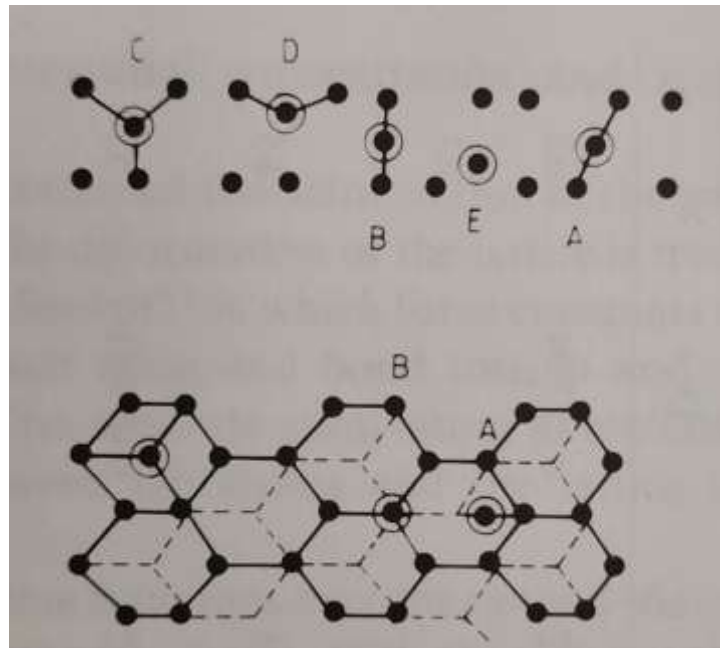


Figure 11 interstitial configurations in graphite

The formation energy of interstitials contains;^[3]

E_s Sublimation energy and it is well known.

E_g The self-energy of the interstitial; the energy required to insert the atom into the crystal lattice, E_p is the formation energy of carbon atom to the valence state, and E_b is the binding energy of the atom to the lattice.

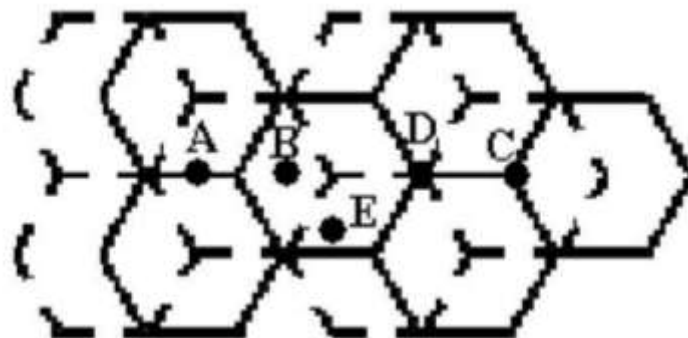
Considering interstitials in bulk graphite. The high symmetry sites of interstitials are labeled as for the adatom in Fig. 10. Site A is the bridge site above a bond center, site C is above an atom in one layer and above a hexagon center in the other layer, while site D is directly between an atom in both adjacent layers.

The formation energies depend strongly on the position of an interstitial atom. E_f is correlated with the number of bonds an interstitial forms with the carbon atoms in the layer. The most stable, high-symmetry site smallest

In site E, the interstitial forms four bonds, of length 1.48 Å and 1.53 Å, two to each layer, as in Fig. (12) f. The next stable high-symmetry site is site A. Here, as in Fig. (12) a, the interstitial sits away from the center of the interlayer and it forms two bonds to one layer of lengths 1.5 Å and 1.6 Å, and two bonds to the other layer both of 1.5 Å.

Allowing the E interstitial to relax in all three directions, we obtain the site with the lowest formation energy in unsheared graphite, denoted F or free. The F interstitial makes two

bonds with a length of 1.48 and 1.52 Å to the layer above and below the interstitial, respectively; see Fig. (12) g. Within the ab plane the relaxed interstitial is close to the high-symmetry site E, but moved slightly out of the center of the triangular towards the D position, as can be seen in Fig. (12) h. The F interstitial in unsheared graphite and the A and E high-symmetry sites all have a formation energy below 7 eV. In these three configurations, the interstitial forms four bonds of similar length 1.5 Å. Site C is the next high-symmetry site in order of increasing formation energy with $E_f = 6.7\text{--}7.3$ eV depending on the exchange-correlation functional and the type of the basis set. In this site the interstitial moves towards the carbon atom above it and pushed this atom out of the graphite layer; see Fig. (12)c. The interstitial forms three bonds with length 1.56 Å; the angles between the interstitial-layer-atom bonds are 97°. Sites B and D have the highest formation energies of all high-symmetry positions. In both sites the interstitial forms only two strong bonds. In site B, Fig. (12) b, the added atoms binds to its nearest neighbors in one layer with bond lengths of 1.52 and 1.62 Å. In site D the interstitial has two bonds of length 1.44 Å to the atoms above and below; the distance to two of its second neighbors decreased from 2.2 Å to 1.75 ± 0.05 Å; see Fig. (12) d. In site D the graphite layers above and below the interstitial are strongly strained. The two carbon atoms directly above and below the interstitial moved out of their high-symmetry positions in the ab plane; see Fig.(12)e. The angle between the two short bonds between the interstitial and its two neighbors thereby decreased from 180° to 165°. The formation energies depend closely on the numbers of bonds formed by the interstitial. Sites E and A form four bonds, two to the layer above and two to the layer below the interstitial. This configuration has been called a spiro by Telling and others, 11 so-called because of its resemblance to the core of the molecule spiro-pentane. The lowest energy interstitial configuration of high symmetry is E and the diffusion path passes over site B. This corresponds to a migration energy of more than 1.5 eV 1.7 eV and it is known that the lowest energy interstitial site has a low symmetry.



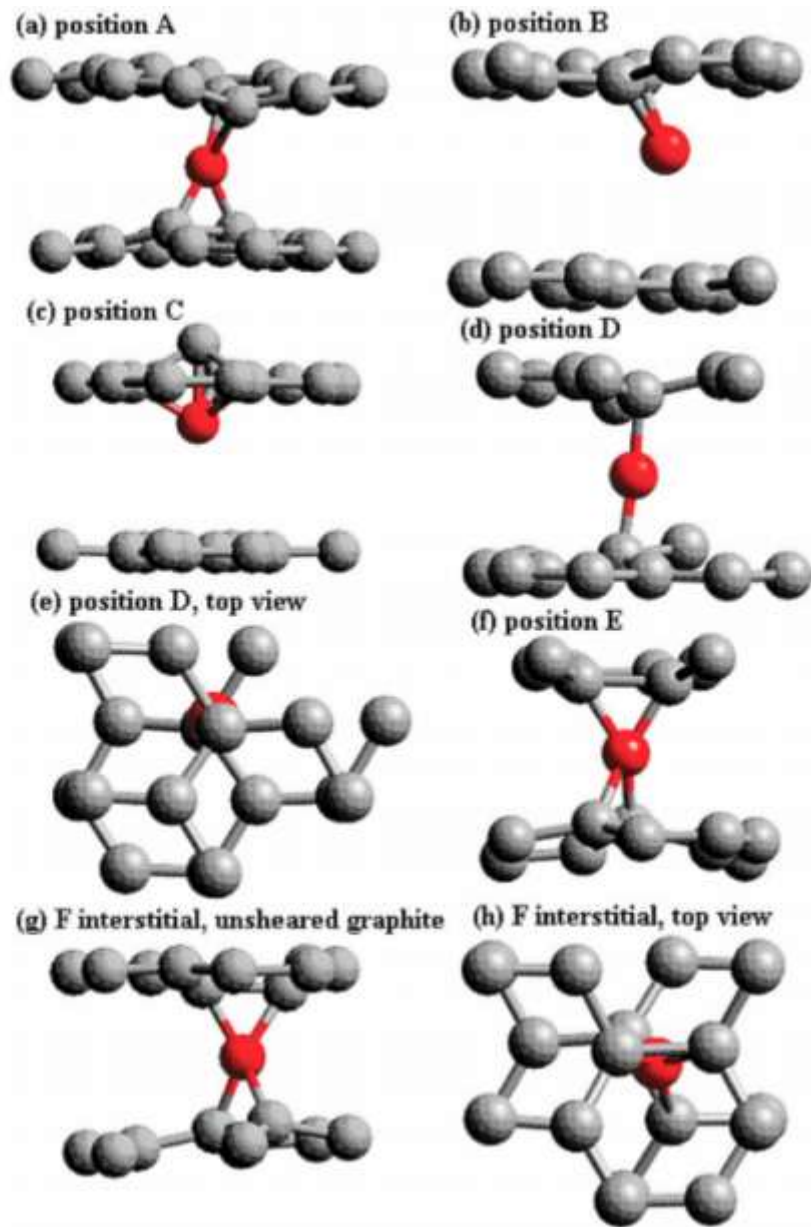


FIG. 12 Light gray atoms are part of graphite; the interstitial is shown in dark red.

2.7.2 SHEARED INTERSTITIALS

As the interlayer bonds are weak so the shear energy of graphite layers is very small, and it has been found that the interlayer interstitials are stabilized when the graphite layer is allowed to shear with respect to the adjacent layers. The sheared interstitial differ from the simple interstitial that it allows the atom to bond to more atoms in adjacent layers and also attract the layers slightly to do this.

The sheared cell is schematically shown in the right side of Fig. (13) a. The interstitial makes four bonds with the layers above and below. The bond lengths are 1.50 Å in this configuration, about 5% larger than in bulk graphite. The second configuration for a shear is half a bond length in a bond direction Fig. (13)b. This shear allows the formation of the ylid interstitial. The ylid is so called because of the y arrangement of bonds around the interstitial, two bonds to one layer and one bond to the opposite layer within a vertical plane. The bond lengths in this case are 1.45 Å. The strong bonds to both layers have caused the layers to move together around the interstitial.

The third configuration occurs for a shear ,shown in the right panel in Fig.(13)c. The interstitial then forms a so-called spiro configuration in which it forms four bonds, two to each layer. This site is the most stable of the interstitials, having a formation energy of only 5.3 eV. This energy is nearly 1 eV below that of the most stable simple interstitial. In this case, the bond lengths are 1.48 Å as shown in Fig.(13)c. Again, the graphite layers have been brought together to achieve these shorter lengths. The last two configurations have cross links between neighboring graphite sheets.

Segregating at the dislocation core gives interstitials with lower energies. Comparing with the cross links in the perfect graphite, they are much more stable in the dislocated graphite. Nevertheless, the energy differences between the lowest-energy, Spiro configuration and the less stable bridge and ylid configuration are similar to unsheared graphite, $E_f(\text{sheared}) \geq 1.4$ eV, and $E_f(\text{unsheared}) \geq 1.5$ eV.

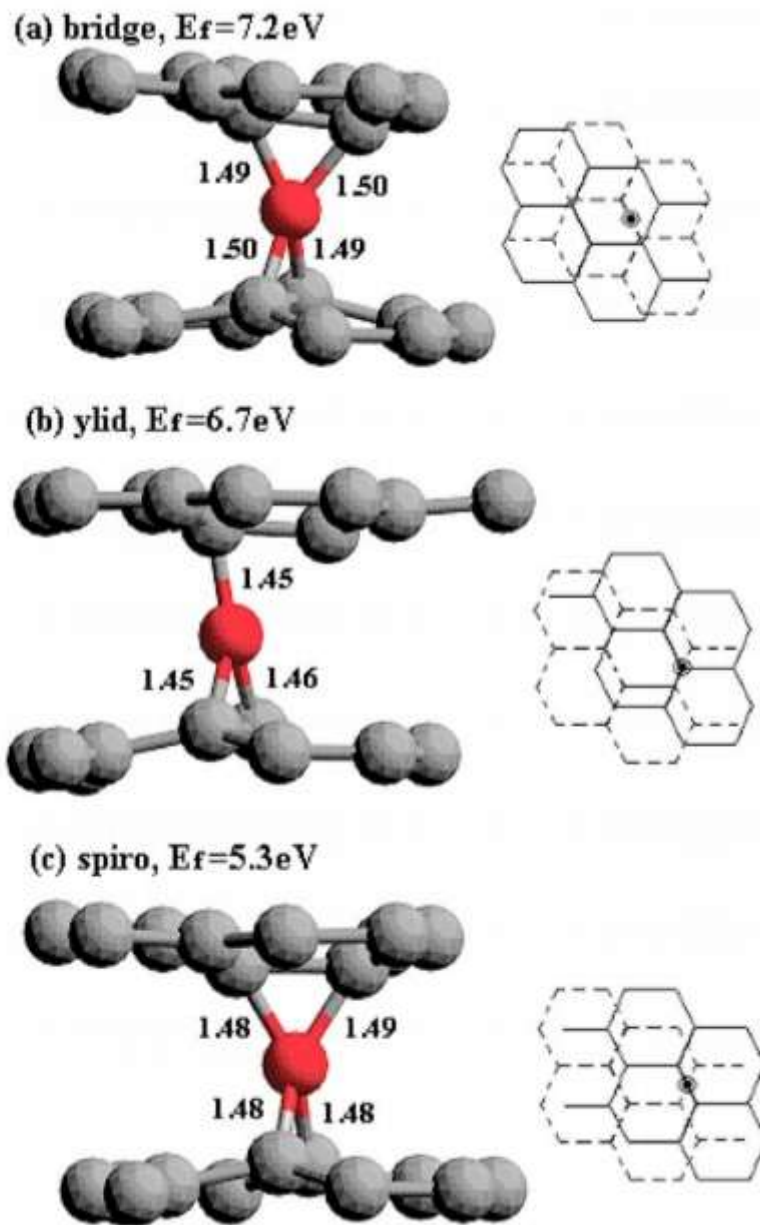


FIG. 13 Three interstitial structures in sheared graphite; a) bridge, b) ylid, and c) spiro The interstitial atom is shown in dark red; graphite is shown in light gray.

2.7.3 VACANCIES

Figure 14 shows the simple lattice vacancy, although it should be noted that in the ABAB lattice sequence the nearest atoms to the basal planes are not energetically equivalent, the energy difference is small compared to the ones involved in the breaking of the nearest neighbor bonds.

Normally the factors taken into account to calculate the vacancy formation energy are the following,^[3]

1. Rupture of the three nearest neighbor or σ -bonds
2. loss of energy of the mobile π -electrons
3. Interaction of the σ -electrons remaining at the vacancy.
4. Rebonding of displaced atom to the crystal surface
5. Rupture of the interlayer Van Der Waals forces.
6. Relaxation of the lattice.
7. Sublimation energy, which is known experimentally to be 7.4 eV

$$E_{fv} = (3E_{\sigma} + \Delta E_{\pi} + 2E_c - E_v) - E_{vs} - E_s \quad (2.5)$$

$$E_s = \frac{3}{2}E_{\sigma} + E_{\pi} + E_c - E_{vs} \quad (2.6)$$

Where E_{σ} is the energy needed to break one σ -bond ;

E_{π} is the π -electron dissociation energy

E_c is the interlayer energy

E_{vs} is the difference in energy between the $3p$ ground state of a free carbon atom and the valence state

ΔE_{π} is the change in the π -electron energy on removing an atom

E_v is the stabilization energy

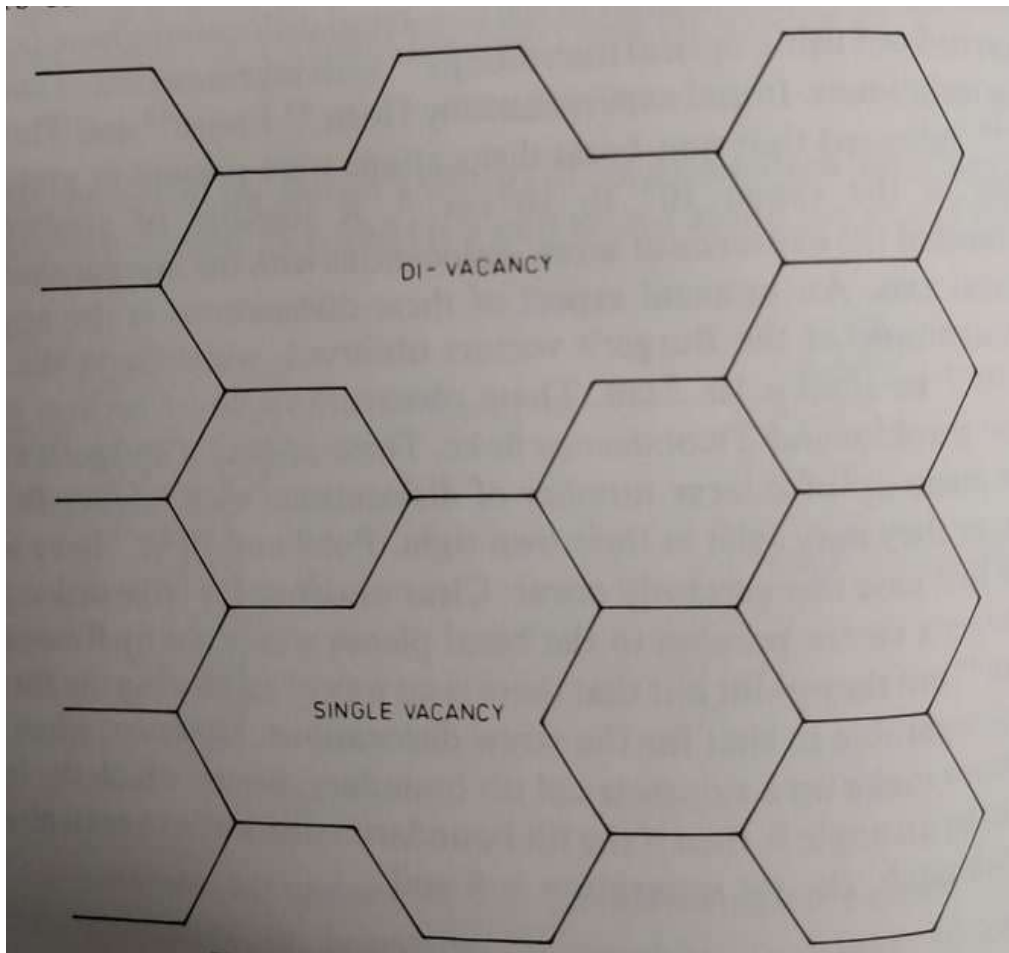


Figure 14 The simple Vacancies in graphite lattice

Bacon and Nicholson carried out a molecular defect model calculation of the single vacancy in graphite, examining positive, negative and neutral vacancies. Neutral vacancy was found to be -11×10^8 eV/cm and gives relaxation energy of 3.32 eV, and the force in the relaxed positions is -14×10^8 eV/cm, these forces are used to make interaction between vacancies of the same plane, the vacancy formation area is found to be -0.140 atomic areas.

The hexagonal graphite structure allows there to be two vacancy structures. Vacancy V_{α} consists of a vacancy lying directly above an atom site on the adjacent layers. Its formation energy is calculated to be 7.6 eV. The other configuration V_{β} is a vacancy site lying between centers of hexagonal voids on the planes adjacent to the plane of the vacancy. Its formation energy is found to be 8 eV. These values compare to 7.8 eV found by Kaxiras and Pandey and 7.4 eV by Al-Barbary .

The vacancy atomic configurations and the directions of atomic relaxation are shown in Fig. (15). The three nearest atoms move away from the vacancy and are displaced by about 0.4 Å. The displacement of the more distant atoms is, however, sufficiently smaller. This result contrasts with the results of Xu, where the vacancy's first neighbors move closer to the vacancy and the first and second neighbors are displaced by 0.3 Å. The migration barrier for vacancies is an order of magnitude larger than that of the interlayer interstitials.

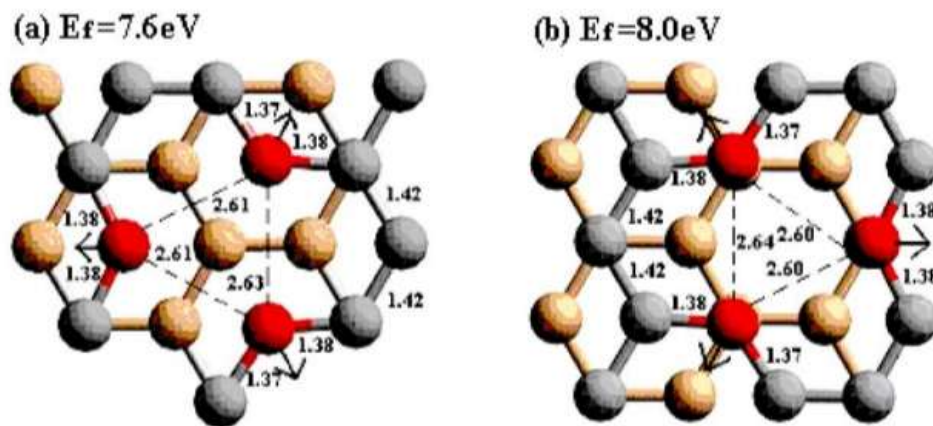


FIG. (15) Two types of vacancies: a) V and b) V. Arrows indicate relaxation directions for the nearest neighbors red of a V. The layer below is light brown.

2.7.4 INTERSTITIAL-VACANCY (I-V) PAIR

Ewels et al found that Vacancies and interstitials may recombine without energy barrier and also have another possibility of forming a I-V bound pair can occur in graphite, depending on the symmetry of the interstitial atom.

An intimate I-V pair is formed as the interstitial and the vacancy interact to form a metastable I-V complex. Its formation energy is calculated to be 10.8 eV. This is a gain in energy of 2.1 eV compared to the most stable isolated interstitial and vacancy configurations, even in sheared graphite. In the most stable form of this complex, the interstitial adopts the ylid structure.

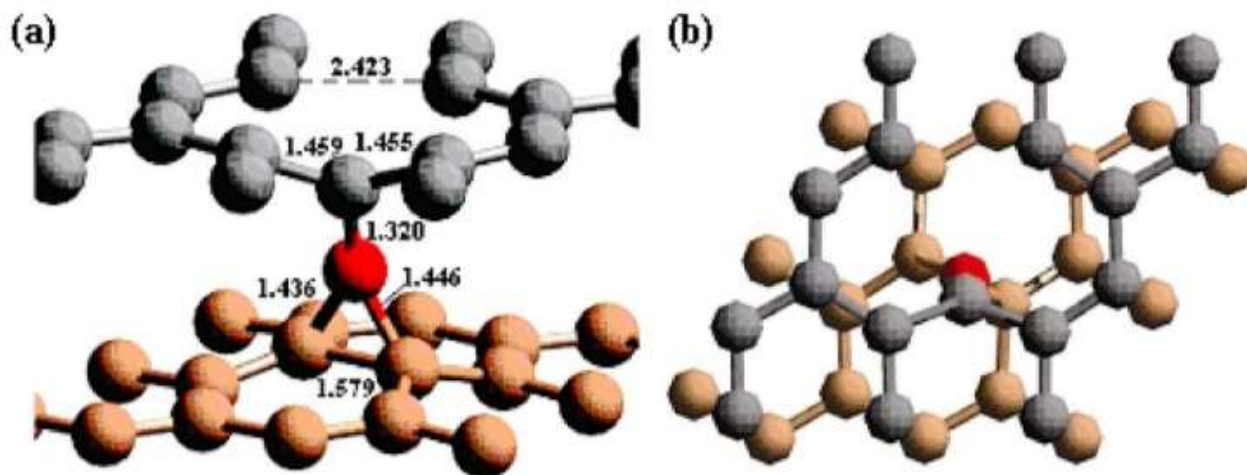


FIG.(16) The intimate I-V pair in sheared graphite a) side view b) top view. The interstitial atom is red; atoms in the sheet below are light brown. Dashed line indicates the weakly reconstructed vacancy bond.

The interstitial atom is bonded to one of the three C atoms surrounding the vacancy and also bonds to two C atoms in the sheet below. The two other C atoms around the vacancy form a weakly reconstructed bond. The single bond from the interstitial to the vacancy is extremely short, 1.32 Å, while the other two are 1.44 Å. The short bond is a distorted double bond, which accounts for the stability of this I-V complex. This complex can only recombine into perfect graphite once the recombination barrier of about 1.3 eV is overcome. In unsheared graphite, the interstitial sites are less stabilized. This allows the I-V pairs to recombine without a barrier.

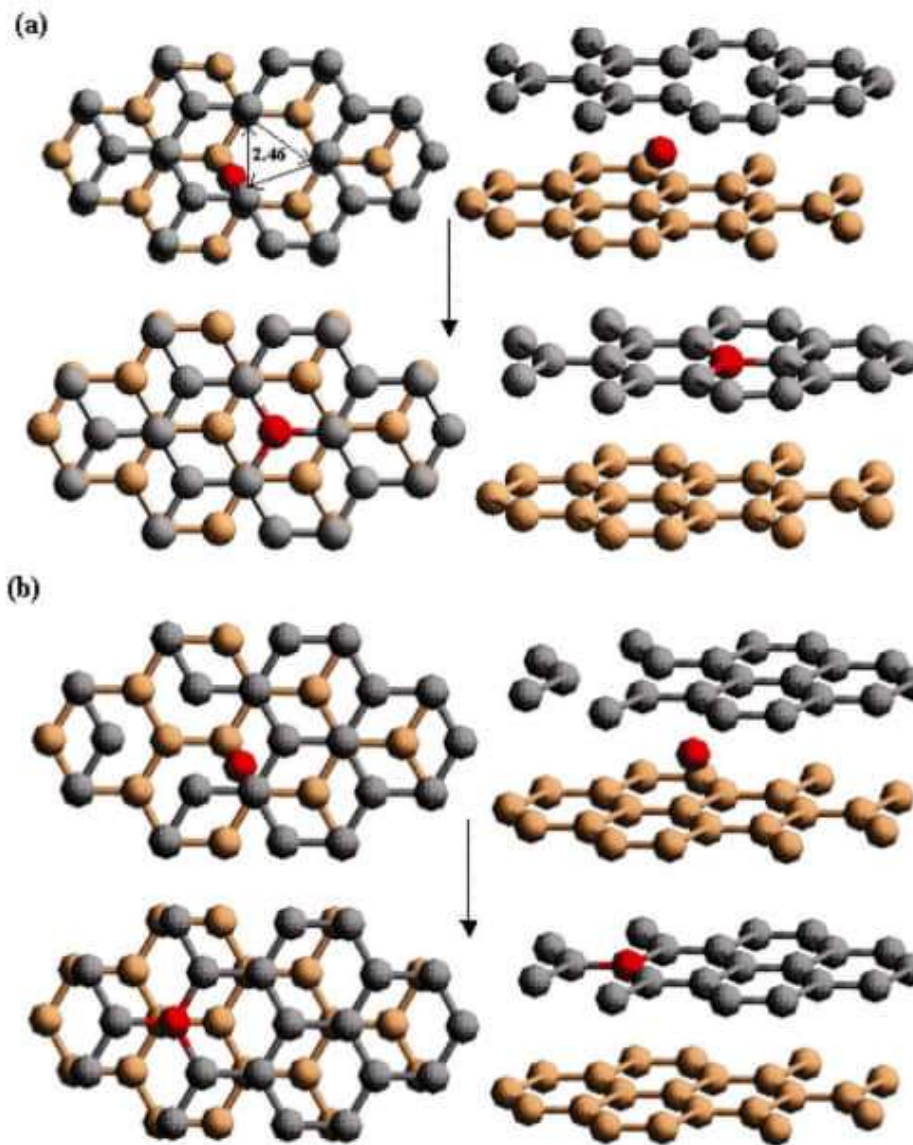


FIG. (17) The recombination process between an interstitial and a vacancy in unsheared graphite; a) I and V and b) I and V.

2.7.5 Stone-Wales Defect

The Stone-Wales SW transformation in a graphite sheet is the rotation of a pair of atoms by 90° to convert four hexagonal rings into two pentagons and two heptagons, as in Figs. 18

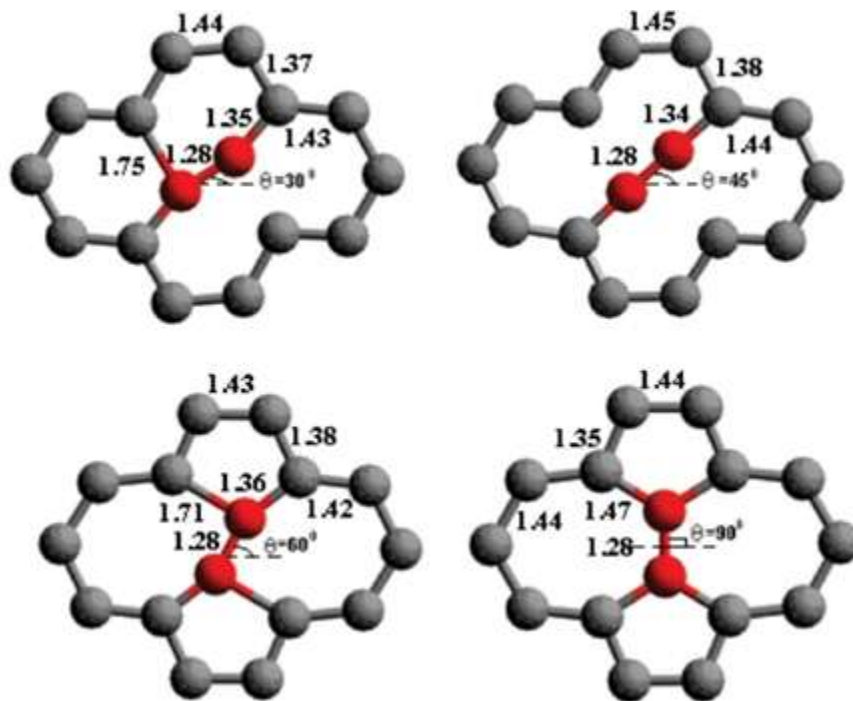


FIG. (18) Stone-Wales defect.

a) In-plane atom pair exchange. The direct-exchange atoms are dark red.

Mechanical Properties of graphite

Graphite defects shown in the previous chapter, will affect its mechanical properties, the grain structure of the graphite affects heavily its mechanical properties, as known there is graphite with fine grains and some medium-grained depending on the method of manufacture as well as the precursor materials used during manufacturing as mentioned in the previous chapter. In fact the fine grained graphite with the known specimen dimension for tensile testing would have grains more than enough compared to the same dimension of the medium grained specimen.^[14] The conventional technique is to use a sample and create a mechanical test on this specimen and subject it to forces like tension, compression, torsion and bending and therefore we can make the calculation of the stress and strain from the measured forces and displacements. Most of the experiments are done on large graphite sample as single crystals are too small for the mechanical test techniques such as Cantilever beams mechanical test is a technique which means a rigid bar that is fixed to support a vertical structure or wall and that beam's other end is free to carry some vertical loads on the free side, so the fixed end has a reaction force and moment created by the load acting on the free end.^[15] Also Single-filament tensile test, resin impregnated tow tensile test which is to provide the tow with sufficient mechanical strength to produce a rigid test specimen which could sustain uniform loading of individual filaments, Stress Rupture, Creep Testing and Charpy V-notch Impact Testing.

In this chapter we will discuss the mechanical properties of graphite which involve two different approaches; macroscopic which consider stress and strain tensors and microscopic which consider the potential energy of elastic deformation of crystal and how to get the elastic modulus of elasticity, rigidity modulus and poisson's ratio, damping factors and the variation of graphite hysteresis loops, creep behavior and the stress alternation impact on the graphite specimens and its effect on the fatigue and the failure point in terms of the temperature of the surroundings and at least the frictional behavior of graphite.

3.1 Density.^[13]

Density is a good indication of the perfection of the graphite lattice. The density of the ideal and well-ordered graphite, varies approximately from 2 to 2.265 g/ml according to Hafmann, Wilm and Csalan calculations, on the other hand the density of synthetic graphite is about 1.6 g/ml or lower, usually there are lines indicating closed or open pores in carbons, some of these pores are accessible while others are blocked. When the graphite is with low density an irreversible decrease in volume is noticeable on compression due to a breakdown of inter-crystallite bonds.

Graphite is considered as a brittle material which requires considerations of non-uniform stresses. There is a remarkable difference in the atomic binding, especially between the tight binding of atoms in the basal planes themselves due to the existence of the covalent bonds, these differences in the atomic binding affect the elastic, plastic and fracture behavior in mono-crystalline and polycrystalline graphite.^[3]

3.2 The mechanical properties of single crystal graphite.^[3]

First let's introduce the strain tensor ε_{ij} , and the stress tensor σ_{ij} and considering their relationship which in turn characterizes the elastic properties of the graphite. The strain tensor ε_{ij} , which describes the change in shape and volume of a crystal under the action of external forces and it is a symmetric tensor and strain tensor as $\varepsilon_{ij} = \varepsilon_{ji}$, the diagonal components of the tensor ε_{ii} define the tensile or compressive strains in the direction of the three rectangular axes ($i = 1,2,3$), and the off-diagonal components ε_{ij} ($i \neq j$), describe the shearing strain. As the crystal is strained its parts are no longer in equilibrium, hence stresses arise to bring the crystal parts into equilibrium, and these stresses are described by a symmetric tensor $\sigma_{ij} = \sigma_{ji}$, the diagonal stresses describe stresses along the axes and the off-diagonal stresses describe shearing and tangential stresses.

There is a linear relation between strain and stress called Hook's law which is used to express the small deformations which is presented in one of the following forms:

$$\varepsilon_{ij} = S_{ijkl} \sigma_{kl} \quad (3.1)$$

$$\sigma_{ij} = C_{ijkl} \varepsilon_{kl} \quad (3.2)$$

Where the coefficients S_{ijkl} and C_{ijkl} are the elastic compliance and elastic moduli respectively. The strain and stress tensors are replaced by the corresponding vectors in a six dimensional space, while tensors of elastic moduli and elastic compliance are replaced by second-rank tensors in six dimensional space as shown later;

$$\text{where } [\varepsilon] = \begin{bmatrix} \varepsilon_{xx} \\ \varepsilon_{yy} \\ \varepsilon_{zz} \\ \varepsilon_{xy} \\ \varepsilon_{yz} \\ \varepsilon_{zx} \end{bmatrix} \text{ and } [\sigma] = \begin{bmatrix} \sigma_{xx} \\ \sigma_{yy} \\ \sigma_{zz} \\ \tau_{xy} \\ \tau_{yz} \\ \tau_{zx} \end{bmatrix} \text{ and } [S] = \begin{bmatrix} S_{11} & S_{12} & S_{13} & S_{14} & S_{15} & S_{16} \\ S_{21} & S_{22} & S_{23} & S_{24} & S_{25} & S_{26} \\ S_{31} & S_{32} & S_{33} & S_{34} & S_{35} & S_{36} \\ S_{41} & S_{42} & S_{43} & S_{44} & S_{45} & S_{46} \\ S_{51} & S_{52} & S_{53} & S_{54} & S_{55} & S_{56} \\ S_{61} & S_{62} & S_{63} & S_{64} & S_{65} & S_{66} \end{bmatrix}.$$

Due to the symmetry of elastic constants that their number reduces from 36 to 21, and due to the hexagonal symmetry of graphite, the number of independent elastic constants is five, $C_{11}, C_{12}, C_{13}, C_{33}$ and C_{44} and for hexagonal symmetry it is known that $C_{22} = C_{11}, C_{13} = C_{23}, C_{55} = C_{44}, C_{66} = \frac{1}{2}(C_{11} - C_{12})$, and the remaining elastic moduli are zero, the same for the elastic compliance S_{ij} .

The tensor of the elastic moduli for graphite is written in the form of the following matrix:

$$C_{ij} = \begin{pmatrix} c_{11} & c_{12} & c_{13} & 0 & 0 & 0 \\ c_{12} & c_{11} & c_{13} & 0 & 0 & 0 \\ c_{13} & c_{13} & c_{33} & 0 & 0 & 0 \\ 0 & 0 & 0 & c_{44} & 0 & 0 \\ 0 & 0 & 0 & 0 & c_{44} & 0 \\ 0 & 0 & 0 & 0 & 0 & c_{66} \end{pmatrix}.$$

These relations are valid in hexagonal between C_{ij} and S_{ij} :

$$C_{11} + C_{12} = S_{33}/S, \quad C_{13} = -S_{13}/S, \quad C_{33} = (S_{11} + S_{12})/S, \quad C_{44} = 1/S_{44}, \quad C_{66} = 1/S_{66} \quad (3.3)$$

And

$$S = S_{33}(S_{11} + S_{12}) - 2S_{13}^2 \quad (3.4)$$

The elastic constants are defined in several ways by empirical relations between stress and strain or by an expansion of the energy per unit volume in terms of applied strain. It's known that the deformation of any body can be described by six independent strains in a Cartesian coordinates as W is the strain energy, in a unit cube subjected to 6 independent strains e_{lm} may be expanded as the series

$$W = W_o + \sum_{lm} \left(\frac{\partial W}{\partial e_{lm}} \right) e_{lm} + \frac{1}{2} \sum_{lm, no} \left(\frac{\partial^2 W}{\partial e_{lm} \cdot \partial e_{no}} \right) e_{lm} \cdot e_{no} + \frac{1}{6} \sum_{lm, no, pq} \left(\frac{\partial^3 W}{\partial e_{lm} \cdot \partial e_{no} \cdot \partial e_{pq}} \right) e_{lm} \cdot e_{no} \cdot e_{pq} + \dots$$

Where W_o is the energy/unit volume in the unstrained state. The differential coefficients are evaluated at zero strain and the term $\left(\frac{\partial W}{\partial e_{lm}} \right)$ must be zero in this condition. The symmetry of the crystal limits the number of independent differential coefficients to 5 for the second term and 10 for the third term.

One of the standard equations relating stress and strain for a hexagonal crystal

$$e_{xx} = S_{11}T_{xx} + S_{12}T_{yy} + S_{13}T_{zz} \quad (3.5)$$

e_{lm} are the strains in a Cartesian coordinate system with the z-axis parallel to the hexagonal axis of the crystal (c-axis). T_{lm} are the stresses which is the force acting on the unit area parallel to the normal to the l th direction, the normal to the unit area which is in the m th direction.

The universal relationship of stresses to strains is

$$T_{xx} = C_{11}e_{xx} + C_{12}e_{yy} + C_{13}e_{zz} \quad (3.6)$$

As mentioned S_{ij} are the elastic compliances and C_{ij} are the elastic moduli, The Young's moduli and shear moduli as measured conventionally are related to S_{ij}

Young's modulus parallel to the hexagonal axis.

$$E_c = S_{33}^{-1} \quad (3.7)$$

Young's modulus parallel to the basal planes,

$$E_a = S_{11}^{-1} \quad (3.8)$$

Shear modulus parallel to the basal planes,

$$G = S_{44}^{-1} = C_{44} \quad (3.9)$$

Shear modulus of individual layer

$$G = \frac{1}{2}(S_{11} - S_{12})^{-1} = \frac{1}{2}(C_{11} - C_{12}) \quad (3.10)$$

The young's modulus E is measured in the direction making an angle ϕ with the hexagonal axis is given by

$$\frac{1}{E} = S_{11}(1 - \gamma^2)^2 + S_{33}\gamma^4 + (2S_{13} + S_{44})\gamma^2(1 - \gamma^2) \quad (3.11)$$

Where $\gamma = \cos \phi$.

The variation of the Young's modulus with ϕ , obtained using the best available values of the elastic constants as shown in figure 18 a, this figure shows, In the also same way the rigidity modulus G measured on a cylinder oriented along ϕ is given by

$$\begin{aligned} \frac{1}{G} = S_{44} + (S_{11} - S_{12} - \frac{S_{44}}{2})(1 - \gamma^2)^2 \\ + 2(S_{11} + S_{33} - 2S_{13} - S_{44})\gamma^2(1 - \gamma^2) \end{aligned} \quad (3.12)$$

The variation of this modulus with angle is shown in figure 20. figure 19 also shows the same relations with all $S_{ij} = 0$ except S_{44} . As this term is dominant for most orientations.

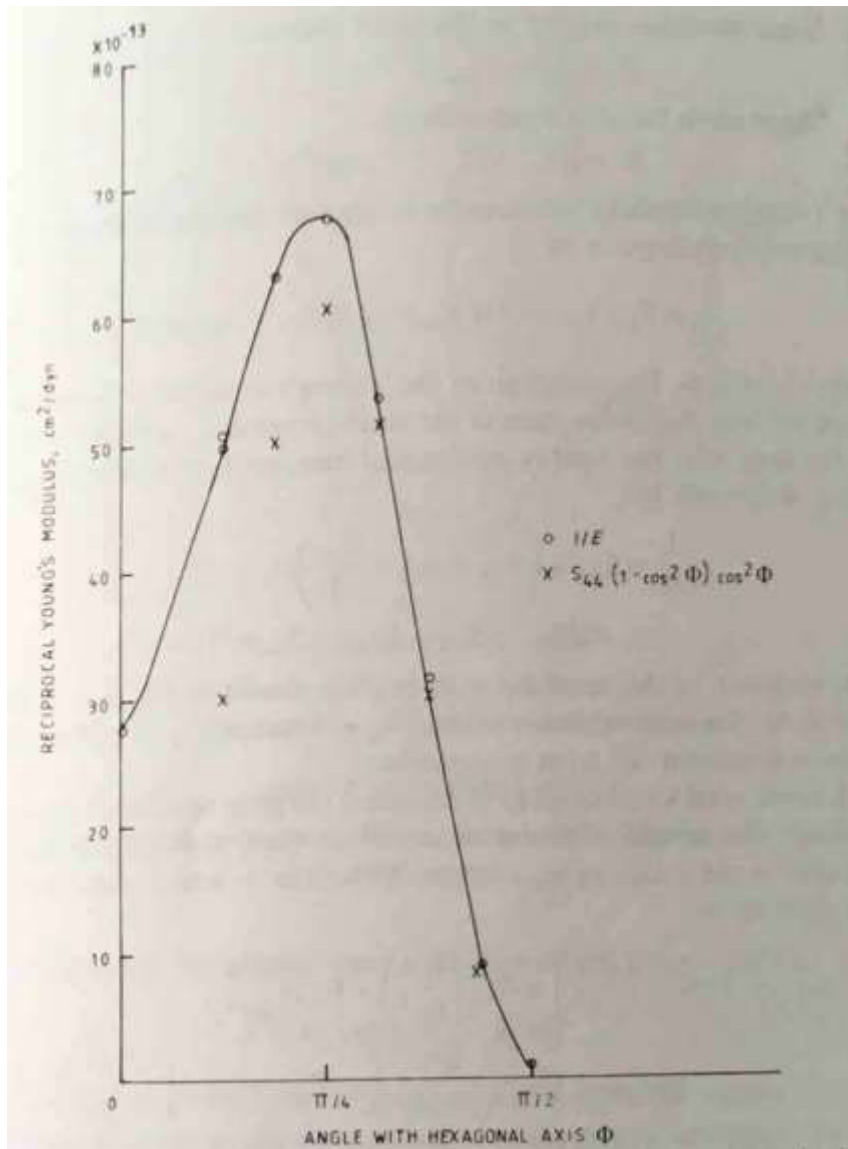


Figure 19 Variation of reciprocal Young's modulus with angle to hexagonal axis in a graphite crystal

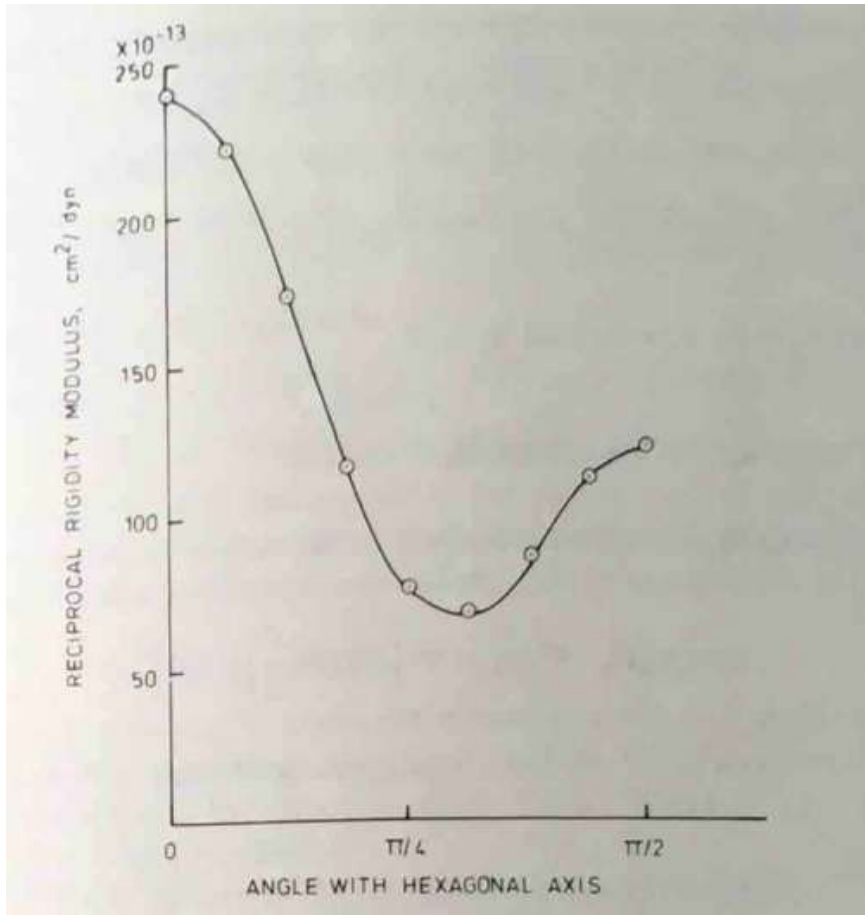


Figure 20 Variation of reciprocal rigidity modulus with angle to hexagonal axis in a graphite crystal

Bowman and Krumhans have discussed the propagation of elastic waves through the crystal. The equations of motion, denoting displacement parallel to the z-axis by w , and parallel to the x and y axes by u and v , and concluded the equations with a plane wave solutions of the form:

$$A = A_0 \exp[i(\omega t - \mathbf{K} \cdot \mathbf{r})] \quad (3.12)$$

Where $A_0 = u_0 \mathbf{i} + v_0 \mathbf{j} + w_0 \mathbf{l}$; \mathbf{r} is the position vector and \mathbf{K} the wave vector, ω is the circular frequency, t the time and \mathbf{i}, \mathbf{j} and \mathbf{l} are orthogonal unit vectors. Substitution of this solution into the equations of motion gives the simultaneous equations

$$\rho_0 \omega^2 u_0 = (C_{11} K_x^2 + C_{66} K_y^2 + C_{44} K_z^2) u_0 + (C_{66} + C_{12}) v_0 k_x k_y + (C_{44} + C_{13}) w_0 k_x k_z$$

$$\rho_0 \omega^2 v_0 = (C_{66} K_x^2 + C_{11} K_y^2 + C_{44} K_z^2) v_0 + (C_{66} + C_{12}) u_0 k_x k_y + (C_{44} + C_{13}) w_0 k_x k_z$$

Where $k_x = lk, k_y = mk$ and $k_z = nk$

After the solution of these equations they get longitudinal wave and transverse waves, then there were several attempts to measure the elastic constants C_{xy} of single crystal graphite. Baker and Kelly measured the resonant frequencies of cantilever beams, the beams were cut from the Ticonderoga flakes with their long direction parallel to the basal planes and the beam thickness parallel to the hexagonal axis. The relatively small ratio C_{44}/C_{11} for graphite requires a solution of the motion equations of the cantilever which takes account of shear deformation and the normal bending stresses. The complete equation has two limiting solutions:

1. If the deformation is dominated by shear the resonant frequency is

$$f = \frac{1}{4l} \left(\frac{C_{44}}{\rho_0} \right)^{1/2} \quad (3.13)$$

where l is the length.

2. If the deformation is dominated by bending, the resonant frequency is

$$f = \left(\frac{Et^2}{12\rho_0} \right)^{1/2} \frac{(1.875)^2}{2\pi l^2} \quad (3.14)$$

Where $E = S_{11}^{-1}$

After several studies, it was indicated that the true crystal value of C_{44} ranging between 4 to 4.5 dyn/cm^2 , and the presence of glissile basal plane dislocations can reduce this by one or two orders of magnitude value.

The compressibility is $k = 2(S_{11} + S_{12}) + S_{33} + 4S_{13} \approx S_{33} + 4S_{13}$, and The experimental value of compressibility of Ceylon graphite at the room temperature and at zero pressure Bridgeman found it to be $298 \times 10^{-14} \text{cm}^2/\text{dyn}$ and decreasing with increasing pressure, Basset has found that natural graphite was considerably more compressible as was a Ceylon graphite and an Acheson synthetic graphite.

Drickamer et al used X-ray techniques to measure the hydrostatic compressibility figure 21 shows Drickamer data which agrees with Bridgeman, it must be noted that the zero pressure measurements of elastic constants are incompatible with high pressure measurements of Drickamer and others.

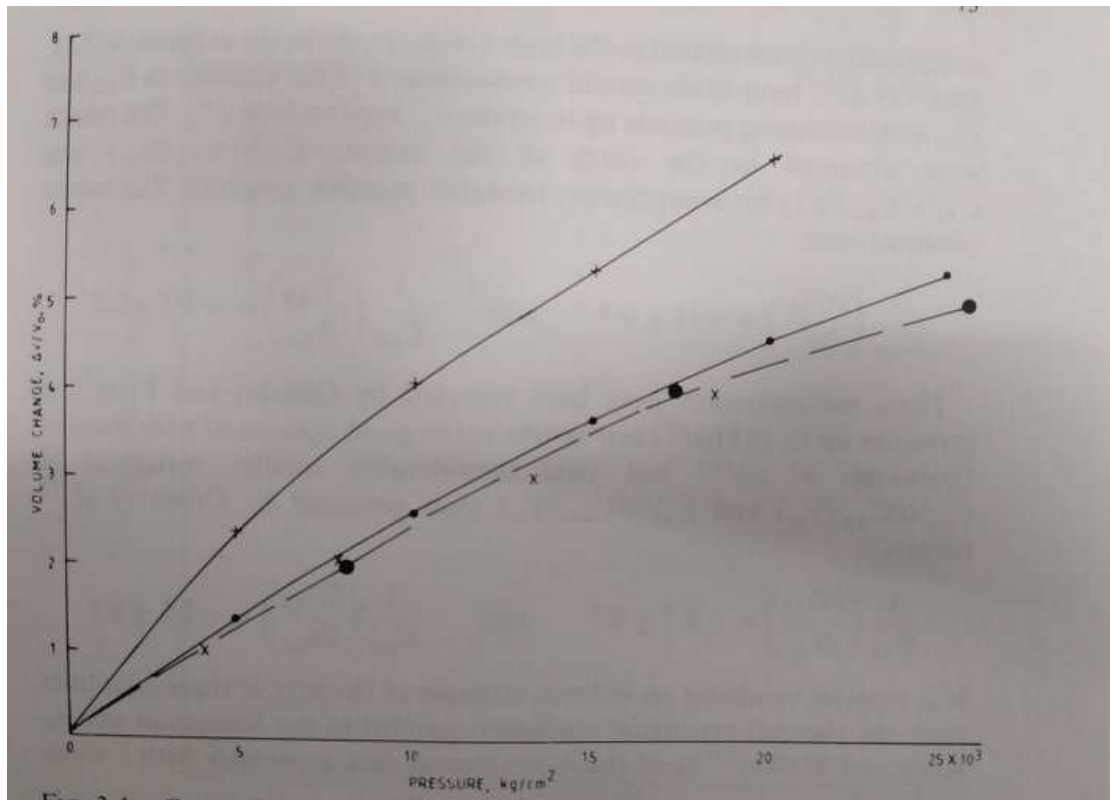


Figure 21 comparison of data for graphite compressibility + Basset , X
 Gauster, small black dot • Bridgement, larger black dot ● Drickamer
 et al.

The union carbide workers determined the stress-strain relations at finite stresses on both natural crystals and highly oriented pyrolytic graphite. The pyrolytic graphite has a linear stress-strain curve under all stresses except basal shear. The natural single crystals were tested in shear only and showed non-linear stress-strain curves.

In the single crystal material an initial linear stress-strain curve is almost flat, easy glide region. The intersection of these is the critical yield stress σ_c . The yield stress is sensitive to previous history of the crystal the average value for the Ticonderoga flakes was found to be $0.29 \times 10^6 \text{ dyn/cm}^2$, while in unstrained crystals values are low as $0.15 \times 10^6 \frac{\text{dyn}}{\text{cm}^2}$.

3.3 The elastic constants of polycrystalline graphite.^[3]

Many authors have studied the stress-strain curve in tension and compression, Losty and Orchard have showed the non-linearity of transverse strains. The dependence of the elastic properties on temperature is also complex with variations from on graphite to another. At low temperatures the moduli decrease with increasing temperature as expected thermodynamically, but at room temperature it's its minimum value and then increase up to about 2000°C and then decrease once more, it's also shown that the dynamic elastic moduli (maximum strain $\leq 10^{-4}$) are always greater than those at small but finite strain up to 2500°C.

The deformation of a polycrystalline body is described by five elastic moduli or compliances. In a co-ordinate system with z-axis coinciding with the symmetry axis, the relationship between stress F_{ij} and strain E_{cm} is written as:

$$\begin{aligned}
 E_{xx} &= S_{11}F_{xx} + S_{12}F_{yy} + S_{13}F_{zz} \\
 E_{yy} &= S_{12}F_{xx} + S_{11}F_{yy} + S_{13}F_{zz} \\
 E_{zz} &= S_{13}(F_{xx} + F_{yy}) + S_{33}F_{zz} \\
 E_{zx} &= S_{44}F_{zx} \\
 E_{zy} &= S_{44}F_{zy} \\
 E_{xy} &= 2(S_{11} - S_{12})F_{xy}
 \end{aligned} \tag{3.15}$$

And

$$\begin{aligned}
 F_{xx} &= C_{11}E_{xx} + C_{12}E_{yy} + C_{13}E_{zz} \\
 F_{yy} &= C_{12}E_{xx} + C_{11}E_{yy} + C_{13}E_{zz} \\
 F_{zz} &= C_{13}(E_{xx} + E_{yy}) + C_{33}E_{zz} \\
 F_{zx} &= C_{44}E_{zx} \\
 F_{zy} &= C_{44}E_{zy} \\
 F_{xy} &= 2(C_{11} - C_{12})E_{xy}
 \end{aligned} \tag{3.16}$$

This relations are only strictly true in polycrystalline graphites for very small strain, since the apparent elastic constants are strain dependent.

It was observed that the elastic modulus was always higher on cooling on the part of the curve where the modulus increased with temperature, also according to Bortz and Lund the maximum of the modulus decreased with increasing numbers of cycles. Andrew and Sato showed that the more graphitized the material the more the modulus increased by temperature, these variations of modulus with temperature are based on the belief the crystals show normal dependence of elastic modulus on temperature. The increase of temperature is caused by changes in the stress distribution due to the closure of microcracks by differential thermal expansions, and it has been noticed that the modulus is affected by the atmosphere most probably in the existence of water vapour. Losty and Orchard showed that the preloading in compression reduces the modulus of elasticity but not the tensile strength and Hall showed that this modulus decrease could be partially recovered by thermal annealing, time at ambient temperature and exposure to fast neutron irradiation. Hart pre-stressed ATJ and AXF graphite in tension and compression up to 40% of failure stress and it was observed that the small strain (dynamic) elastic modulus was reduced in compression the tensile stress reduced the density and thermal expansion coefficient while the compressive stress increased these properties. The modulus changes in AXF graphite were annealed at 1300°C although the recovery was partial in the ATJ graphite. And the results were explained in terms of an increase of dislocation density with crack formation.

Also after three different types of graphite were studied by Oku and Etoin the previous way and it was noticed that small changes occurred in the modulus until the stress exceeded $0.2-0.3\sigma_c$ where σ_c is the compressive strength. Hall pre-stressed ATJ and AXF graphite in tension and compression up to 40% of the failure stress and due to the compressive pre-stressing, strain rate on strength and decrease on young's modulus were observed.

3.4 Theory of elastic constants of polycrystalline graphite.^[3]

For polycrystalline graphite five macroscopic elastic compliance or elastic moduli must be related to five crystal compliances or moduli. All the theories are essentially summarized by the equations:

Macroscopic elastic compliance

$$S'_{ij} = \sum_{lm} a_{ijlm} S_{lm} \quad (3.17)$$

Macroscopic elastic moduli

$$C'_{ij} = \sum_{lm} b_{ijlm} C_{lm} \quad (3.18)$$

The objective of all the theories is to provide values for the coefficients a_{ijlm} and b_{ijlm} and these coefficients are of course inter-related. Voigt and Reuss assumed uniform strains and stresses in an isotropic non-porous body, for the isotropic body there are only three independent constants on the left hand sides of the equation (8). In these simple cases, Markham gives

$$\begin{aligned}
s'_{11} &= \frac{8}{15}S_{11} + \frac{1}{15}S_{33} + \frac{4}{15}S_{13} + \frac{2}{15}S_{44} \\
s'_{12} &= \frac{1}{15}S_{11} + \frac{1}{15}S_{33} + \frac{1}{3}S_{12} + \frac{8}{15}S_{13} - \frac{2}{15}S_{44} - \frac{1}{15}S_{44} \\
s'_{44} &= 2(S_{11} - S_{12}) \\
C'_{11} &= \frac{8}{15}C_{11} + \frac{1}{15}C_{33} + \frac{4}{15}C_{13} + \frac{2}{15}C_{44} \\
C'_{11} &= \frac{8}{15}C_{11} + \frac{1}{15}C_{33} + \frac{4}{15}C_{13} + \frac{2}{15}C_{44} \\
C'_{12} &= \frac{8}{15}C_{11} + \frac{1}{15}C_{33} + \frac{1}{3}C_{12} + \frac{8}{15}C_{13} - \frac{4}{15}C_{44} \\
C'_{44} &= \frac{7}{30}C_{11} + \frac{1}{15}C_{33} - \frac{1}{6}C_{12} - \frac{2}{15}C_{13} + \frac{2}{5}C_{44}
\end{aligned} \tag{3.19}$$

There is another appropriate model for graphite which assumes a non-porous body with a known distribution of crystallites, symmetrically distributed about the extrusion or modeling. In the uniform stress case the relations are now

$$s'_{11} = S_{11} - \frac{1}{2}(2S_{11} + 2S_{13} + S_{44})I_3/I_1 + \frac{3}{8}(S_{11} + 2S_{13} + S_{33} - S_{44})I_5/I_1 \tag{3.20}$$

Where

$$I_n = \int_0^{\pi/2} I(\phi) \sin^n \phi \cdot d\phi \tag{3.21}$$

Where $I(\phi)$ is defined as the density of basal plane normal/unit solid angle at an angle ϕ with symmetry axis and the uniform strain calculation leads in the same way to

$$C'_{11} = C_{11} - (C_{11} - C_{13} - 2C_{44})I_3/I_1 + \frac{3}{8}(C_{11} - C_{13} + C_{33} - 4C_{44})I_5/I_1 \tag{3.22}$$

For the majority of well-crystallised polycrystalline graphite the uniform stress case is most appropriate. With a good approximation

$$s'_{11} = S_{44} \left(\frac{1}{2} \frac{I_3}{I_1} - \frac{3}{8} \frac{I_5}{I_1} \right) \quad (3.23)$$

$$s'_{33} = S_{44} \left(\frac{I_3}{I_1} - \frac{I_5}{I_1} \right)$$

$$s'_{13} = S_{44} \left(-\frac{1}{2} \frac{I_3}{I_1} + \frac{1}{2} \frac{I_5}{I_1} \right)$$

$$s'_{12} = S_{44} \left(\frac{1}{8} \frac{I_5}{I_1} \right)$$

$$s'_{44} = S_{44} \left(1 - \frac{5}{2} \frac{I_3}{I_1} + 2 \frac{I_5}{I_1} \right)$$

An obvious treatment would be to multiply each compliance by a function $F(P)$ of the porosity P . In case of isotropic crystals, for zero porosity

$$\frac{I_3}{I_1} = \frac{2}{3} \quad \frac{I_5}{I_1} = \frac{8}{15}$$

Where

$$s'_{11} = \frac{2}{15} S_{44}$$

$$s'_{12} = -\frac{1}{15} S_{44} \quad (3.24)$$

$$s'_{44} = \frac{6}{15} S_{44}$$

That is E/G in the unusual notation is 3 and the poisson's ratio $\nu = -\frac{1}{2}$, that's quite rare to have a negative Poisson's ratio,^[19] but some materials have this property and are called anti-rubber materials,^[20] which become fatter in cross section when stretched, and called dilational,^[21] arises from the fact that solids with negative Poisson's ratio materials easily

undergo volume changes instead of shape changes, another name for negative Poisson's ratio material is auxetic materials,^[22] which tends to lateral expansion under tension.

3.5 The Damping properties of graphite

Cyclic stressing produces hysteresis loops illustrated in figure 22 the hysteresis increase with the degree of perfection in graphite, the observation of hysteresis loops in graphite crystals associated only with the basal shear mode have led many researchers to accompany the hysteresis of polycrystalline carbons and graphite with basal slip or cracking.^[11]

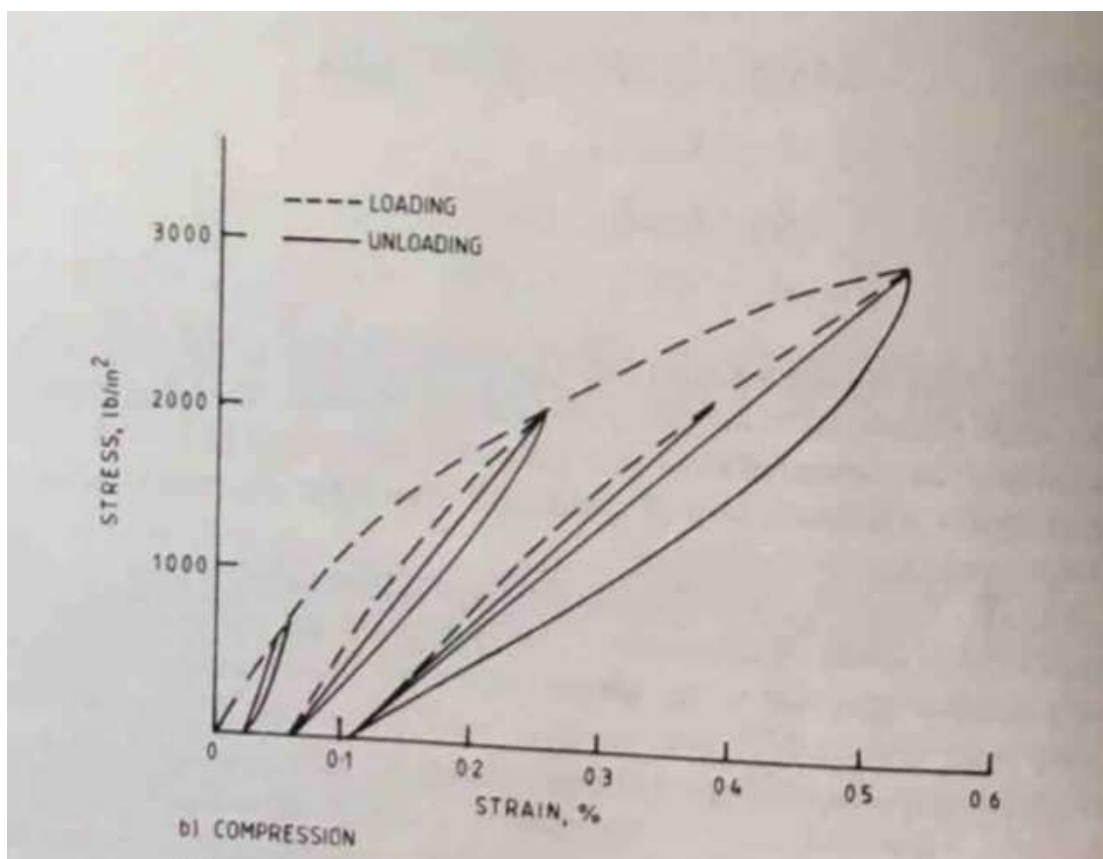


Figure 22 .^[3] Stress strain curve of graphite

The energy lost in a solid subjected to cyclic stresses is known as the damping the small damping is less than 1 , If the energy lost in cycle is ΔW and the energy supplied W , here we introduce λ the logarithmic decrement observed in the free decay of vibrational amplitude, by $\lambda = \Delta W / 2W$. Damping has been observed when measuring the stress and strain curves of graphite which shows the hysteresis loops.

In the finite amplitude measurements the stress and strains within one order of magnitude of the failure stress, the energy loss increases rapidly with strain and the damping values are 0.1.

Early studies of the hysteresis loops were made by Davidson et al and Curry et al the result showed that in a polycrystalline graphite the non-linearity of the stress-strain curve and hence damping increased with heat treatment temperature.

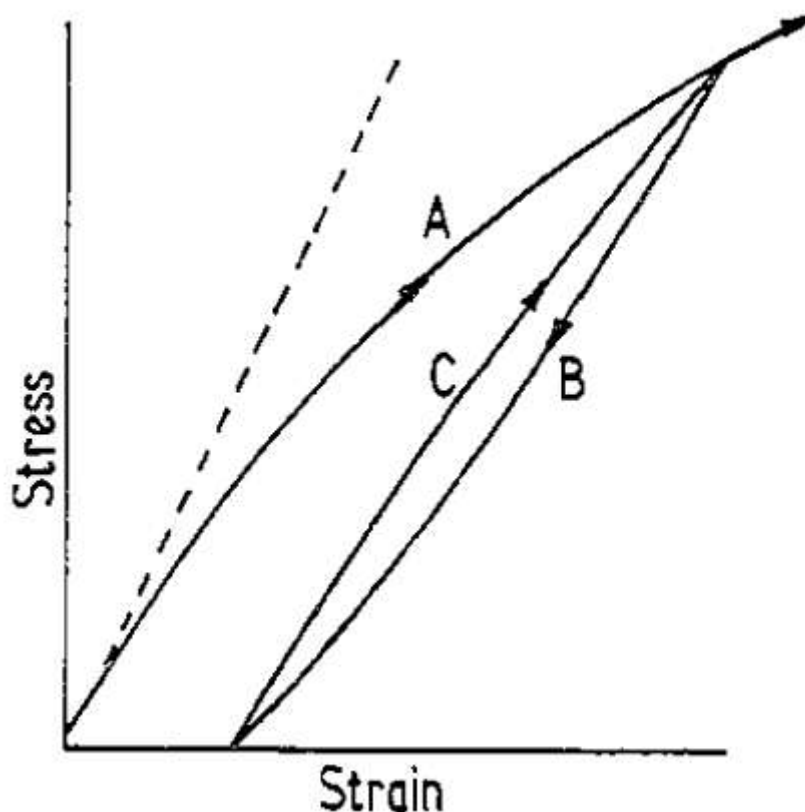


Figure 23.^[12] tension in commercial graphite

The behavior of commercial graphite like reactor graphite under tension stress as seen in figure 21 curve A is never linear when the stress is released permanent set is observed even after small stresses and then after several stresses hysteresis loops are shown in the closed loop between curves B and C. graphite remains in the elastic region while being in these loops cycling between the same stress limits producing superimposed loops. The apparent modulus decreases as the stress range in the cycling increases.

Graphite deforms and finally fractures by sliding along preferred layers by striations within the grist particles, the striations are quite ordered in layers which may plastically by

applying the smallest stress by dislocation movement, such mechanism for deformation would conform very well with the interpretation of mechanical hysteresis.

3.6 Creep in graphite

Polycrystalline graphite also shows less common modes of deformation, the creep at low temperature change conditions, a transient creep associated with the commonly observed permanent set and also a marked creep when the temperature approaches the highest heat treatment temperature.

For a half inch diameter rods heat- treated at 2800°C the creep observed showed a logarithmic dependence on time, it was also noticed that in the bend configuration a deflection in the opposite direction reduced the creep when the original load was restored, repeated working on that sample caused reduction to the creep strain, while the permanent set was observed to increase with time of loading.

Jenkins and Williamson loaded a reactor graphite by a torsional dead-weight load and controlled temperature cycles. In temperature cycles 350-50-350°C it was found that the essentially all of the creep occurs in the first cycle and it was shown that increasing the amplitude of the thermal cycle shows a first cycle strain linearly dependent on the amplitude of the temperature cycle, then they proposed an explanation of the effects in terms of the internal strain generation due to the large differential thermal expansion of the graphite crystallites as the graphite is cycled. This strain is sufficient to bring a fraction of the crystallites to the yield point and these deform under the external load.^[3]

Sleggs and Gray made some measurements of the strain on a number of graphites under compression for a constant temperature cycle the first cycle strain compressive stress was found to be inversely proportional to the dynamic young's modulus, and it was reported by Losty that a large creep strain occurs when the temperature of a loaded sample approaches the maximum heat treatment temperature due to the interaction of the stress with the strains developed in the graphitization process.

Davidson and Losty have published the first studies of significant creep of polycrystalline graphite at temperature between 1000°C and 2000°C and the strain in reactor graphite, pitch coke graphite and natural graphite strain was found to be

$$\varepsilon = \sigma \left[\frac{1}{E_T} + \frac{C}{E_0} \exp\left(\frac{-E_1}{KT}\right) \log_{10} \frac{t}{1} + D t \exp\left(\frac{-E_2}{KT}\right) \right] \quad (3.25)$$

Where σ is the stress, t time in minutes (the term unity in the logarithm donates one minute and the creep strain is that measured after that time)

E_0 and E_T are respectively the young's moduli at ambient and at temperature TK

C is a universal constant and D a constant

E_1 and E_2 are activation energies.

Jenkins has studied the transient creep in a polycrystalline graphite at temperature below 1500°C and the creep strain was found to be linearly related to stress and to vary logarithmically with time and the recovery was found to obey a similar logarithmic time-dependence and it's presented in his paper in terms of dislocations overcoming energy barrier by thermal fluctuations.

Malmstrom et investigated the true high temperature creep and the creep of commercial graphite was measured at temperatures between 2400°C and 3000°C and the result was according to this equation

$$\varepsilon = \frac{\sigma}{E_T} + f_1(\sigma) \ln t \cdot \exp\left(-\frac{E_3}{KT}\right) + f_2(\sigma) t \exp\left(-\frac{E_4}{KT}\right) \quad (3.26)$$

Where f_1 and f_2 are functions of stress and the activation energies E_3 and E_4 lay in the range 3 eV-4.5eV and 4eV-8eV respectively. Recovery occurred when the load was removed to an extent rather less than half the transient creep term.

After several investigations it using different methods it was discovered that this previous equation is the best fit.

Creep in tension and compression studied by Wagner et al at temperatures between 2000°C and 3000°C. The secondary creep rates were expressed as

$$\frac{d\varepsilon}{dt} = K \left(\frac{\sigma}{\sigma_f}\right)^{3.8} \exp\left(-\frac{E_4}{KT}\right) \quad (3.27)$$

Where K is a constant (40 for compression and 4 for tension;

σ_f is the failure stress in the particular mode and E_4 is the activation energy found to be 2eV for compression and 2.5 eV for tension.

These are the conclusions from the creep tests which were run up to 2930°C:

1. The creep rate increases continually with temperature.
2. Pre-heating to temperatures above the test temperature reduces the creep rate at constant stress.
3. About one third of the creep strain at a temperature of 2600°C is recoverable when the stress is removed.
4. There is a direct dependence between the temperature of recovery and the rate of recovery.
5. The high temperature creep is due to two distinct thermally activated process.

And for thermal creep of graphite conclusions made by Green and Zukas:

1. The creep strain increases with time as

$$\varepsilon - \varepsilon_0 = At^n \quad (3.28)$$

2. The creep rate at a given strain is proportional to the applied stress

$$\varepsilon - \varepsilon_0 = A_0 \sigma^m t^n \quad (3.29)$$

$$\frac{d\varepsilon}{dt} = \frac{nA_0^{1/n} \sigma^{m/n}}{(\varepsilon - \varepsilon_0)^{(1-m)/n}} \quad (3.30)$$

m/n is generally in the range 6-10 for graphite.

3. The creep rate depends on the temperature through an exponential term with an activation energy of 9-11 eV
4. When the stress is removed the strain recovers, about one quarter of the total creep strain in a few hours at 2500°C and the activation energy of the recovery is 8.3 eV.

Green and Zukas figure 22 ; have observed that the tensile creep deformation is accompanied with numerous small cracks because of dislocation movement under tensile stress from the crack tip by climb, vacancies flowing from the dislocations to the crack tip or interstitial on the opposite direction, the width of the crack is experimentally 1 to 10×10^{-4} cm, the cracks absorb the vacancies and the dislocations are emitted from the tips and that contributes to the strain.^[3]

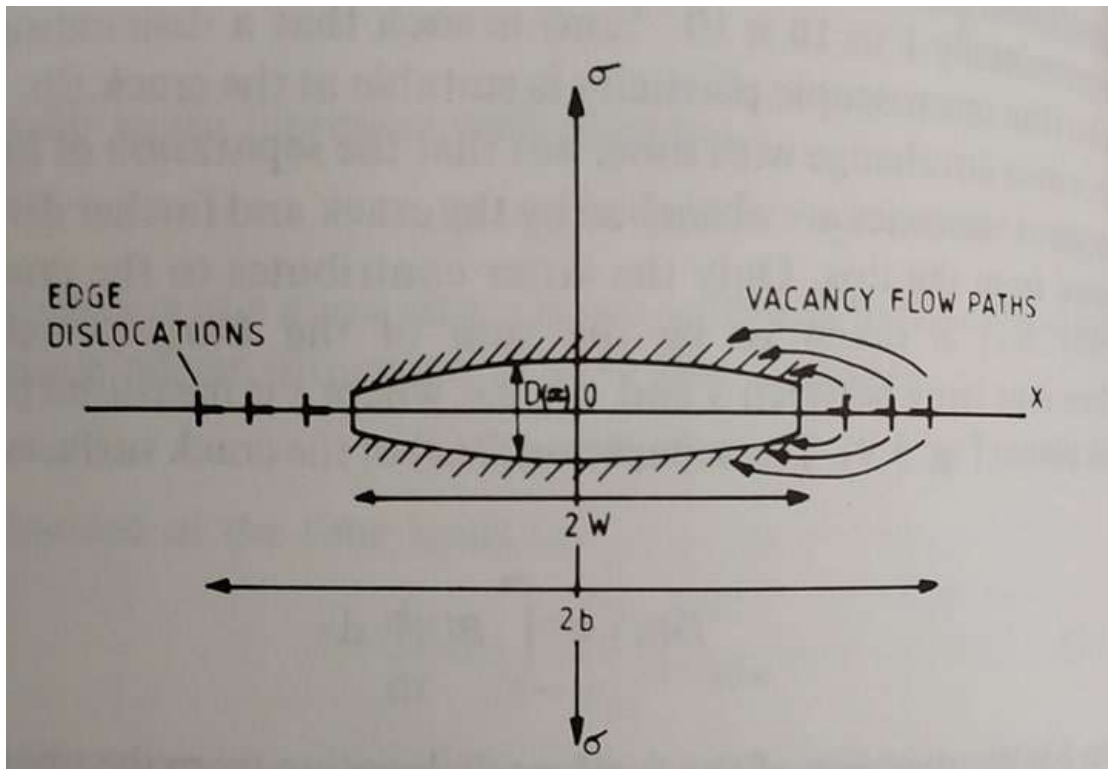


Figure 24 (a) High temperature creep

The creep strain as a function of time

$$\varepsilon - \varepsilon_0 = \left(\frac{2\pi^2 w N \sigma}{3} \right) \left[\frac{D}{N_c \mu K T} \right]^{1/2} t^{1/2} \quad (3.31)$$

N is the density of cracks/unit area

w is the half width

D is the separation of crack

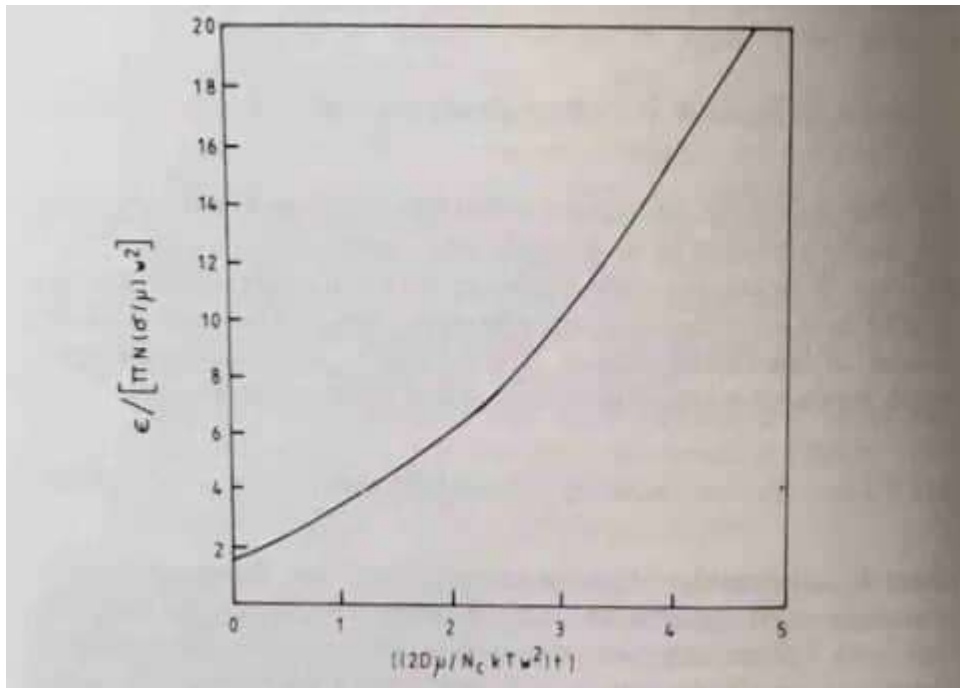


Figure 24 (b) Normalised strain in normalized square root of time

Figure 24 Results of high temperature graphite creep theory

3.7 Fracture of graphite

3.7.1 Highly oriented graphite

The determination of the graphite crystal strength is based on the basal shear strength of Ticonderoga flakes as the crack propagation will be easier along the basal planes than any other crystallographic direction, in figure 25 we can see the propagation of cracks by glide processes.

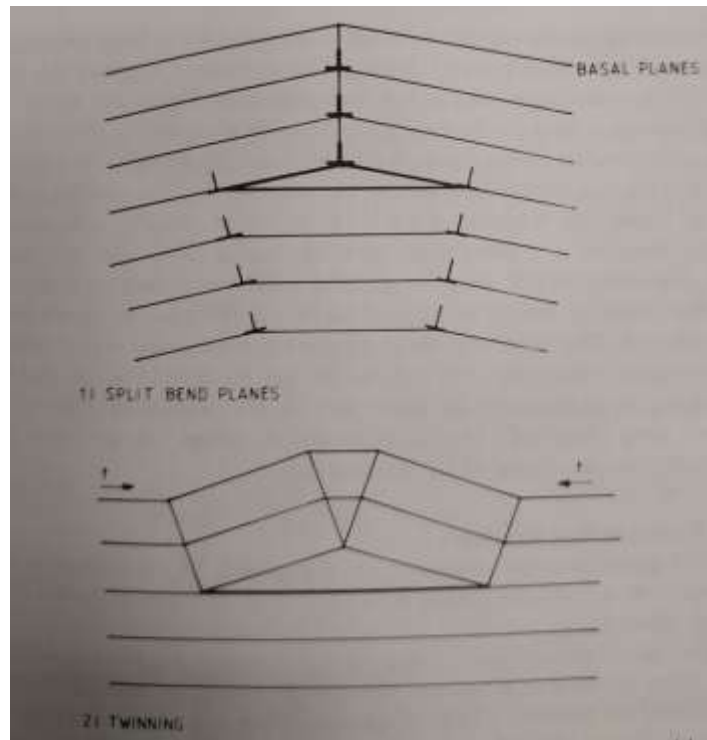


Figure 25 Illustration of crack structures in graphite crystals formed by glide

Soule and Nezbeda repeated shear tests on natural flakes which showed steady increase of the shear strength as the inherent defects were eliminated. The overall value of shear strength is $4.8 \times 10^6 \text{ dyn/cm}^2$ and also the shear tests were repeated on compression annealed pyrolytic graphite but they showed a different behavior unlike the natural flakes, the successive shear measurements showed erratic rather than systematic behavior due to the locking of dislocations by grain boundaries and the shear strength value was $10 \times 10^6 \text{ dyn/cm}^2$

3.7.2 Polycrystalline graphite

when applying a finite stress to polycrystalline carbons and graphites these affects the stress-strain curves and become increasingly non-linear with increasing perfection of the material. The strains at failure are over the whole range of perfection, typical of brittle material that is in pure tension the strain to failure is less than 0.5×10^{-2} , while in compression values obtained are less than 4×10^{-2} . The initial stress- strain relationship is not reversible and the permanent set increases with stress.

One attempt to describe the stress-strain curve after the observation of the hysteresis loops in graphite crystal which is associated only with the basal shear mode, proposed by Jenkins, a model of a stress-induced slipping of elements opposed by frictional forces, that at initial loading $\epsilon = A\sigma + B\sigma^2$ this equation doesn't work if the stress is too large and close to the fracture stress

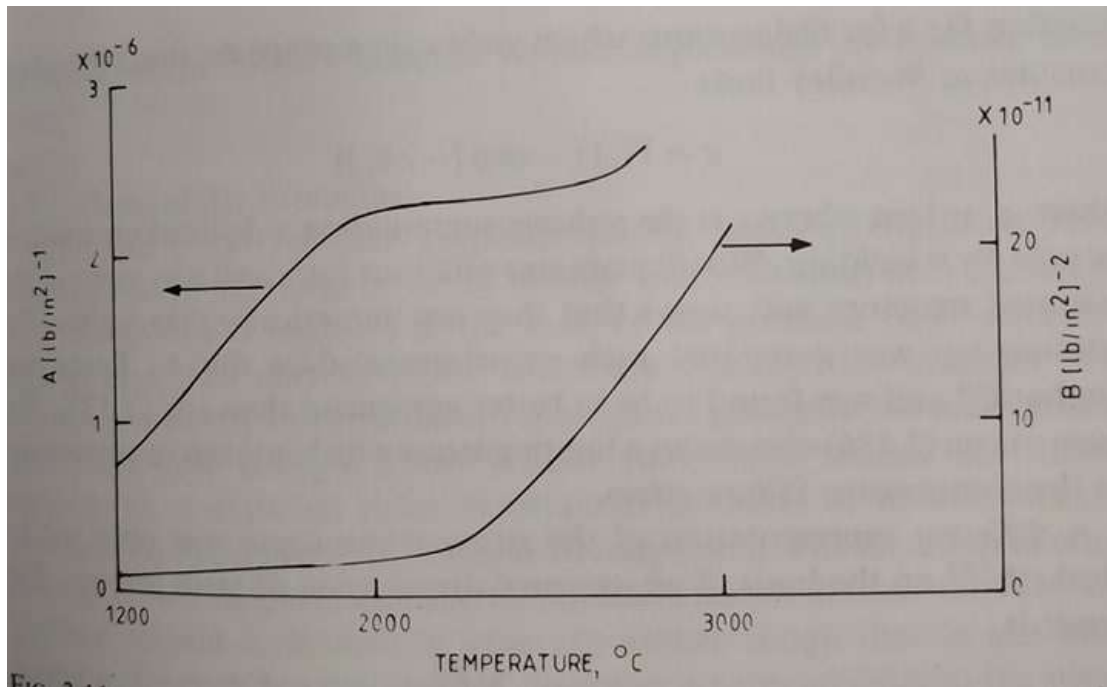


Figure (26) Variation of coefficients A and B with heat-treatment temperature for petroleum coke graphite

When unloading strain $\epsilon_m - \epsilon = A(\sigma_m - \sigma) + \frac{B}{2}(\sigma_m - \sigma)^2$ (3.32)

where ϵ_m is the maximum strain reached on loads of stress σ_m .

At reloading strain $\epsilon - \epsilon_0 = A(\sigma) + \frac{B}{2}(\sigma)^2$ (3.33)

where $\epsilon_0 = \frac{B}{2}(\sigma_m)^2$ this equation doesn't work if the stress to close to the fracture stress.^[3]

3.8 Yielding.^[3]

it's shown in that figure 23 that if the stress is too large of the fracture stress in tension or compression produced changes in the A coefficients due to cracking or new dislocations, individual dislocations can yield to relax the local stress at known stress σ_y and yield strain ϵ_y , if the distribution of dislocations $f(\epsilon_y)$ in a range ϵ_y and took it to be a constant a , Woolley found that the stress considering a model of the basal dislocation structure in the lamellar sub-grains.

$$\sigma = Y\epsilon_0(1 - \exp[-\epsilon/\epsilon_0]) \quad (3.34)$$

where; $\epsilon_0 = 1/va$, where v is the volume around the dislocation which is relaxed by yielding, this equation shows a limiting stress which is taken to correspond to the compressive failure stress.

Hesketh have a different representation of the stress strain curve and assumed the yield

stresses to be

$$\sigma = E\epsilon - \frac{\epsilon^2 E^2}{3.4\sigma_f} \quad (3.35)$$

; where σ_f is the failure stress.

The graphite can slip only in the basal planes, giving two degrees of freedom, rather than the five which are necessary for a crystal to adjust to any deformation and it can show fracture under various combinations of uniform stresses, time-dependent failure and cyclic stress failures.

3.8.1 Quasi- static strengths.^[3]

Polycrystalline graphites shows mean strengths at room temperature which varies from 10 to 30 MN/m² under tension, and the compressive strengths of the same material are generally 3-4 times greater than the tensile strength under similar conditions. As compression has substantial amounts of non-recoverable deformation occur under compression. The fracture surface in tension is rough due to the basic granular structure but the average direction is perpendicular to the stress. In compression it is found that the fracture occurs at 45° to the stress direction.

When applying bi axial stress in the compressive – tensile quadrant, the tensile fracture stress isn't affected by compressive stress until it exceeds the tensile strength, if the compressive stress is large the tensile strength decreases till zero as the compressive stress goes to compressive strength, the strain to failure were reduced by axial tension and increased

by axial compression. Jontner observed that under triaxial stress conditions, the equal compressive stresses in two directions reduces the strength measurements in the third.

The case of graphite was under large hydrostatic stresses with the pressurizing fluid excluded from the pores by a membrane was studied by Kmetko and he showed that under hydrostatic pressure very large reductions in porosity resembling the compression of a sponge were observed, but unlike the large irreversible deformation observed in uniaxial stressing, if the graphite is under hydrostatic stresses, the volume of compaction is reversible, if the confining fluid was allowed to enter through the pores the compression become more linear with pressure and more elastic. Models relating to the existence of the cracks, its growth and its size distribution have been formulated taking into account a homogenous body and slowly variation of the stresses comparing to the size of the crack, and after several models by Weibull the probability of fractions of a material under stress σ is of the form:

$$S(\sigma, V) = 1 - \exp \{-B(\sigma, V)\} \quad (3.36)$$

B depends on the model chosen, S is the shear stress, V is the volume as the failure criteria depends on the graphite dimensions. Then Mayson examined the effect of a sample size taken from an anisotropic nuclear grade graphite on the tensile strength and the results didn't match with the statistical model which expects an increasing strength with decreasing size, and what happened is that the small specimen decrease in strength with decreasing the volume and at larger volumes the predict decrease with increasing volume was observed, this contrast is due to the coarse granular structure of the graphite which contradicts the theoretical assumption.

Brocklehurst found that in the case of isotropic graphite he found an increasing strength with volume up to a peak value is followed by a decrease and also in tension the same increase was observed but then the strength became independent of volume.

In polycrystalline graphites due to the porous the failure is due inherent cracks and the propagation of the cracks condition in a uniform stress field is that the rate of energy released due to spread of the crack should exceed the energy needed to form the new surface and it's

given by

$$\sigma_I = \left(\frac{2E\gamma}{\pi C} \right)^{\frac{1}{2}} \quad (3.37)$$

, where γ is the surface energy/unit area and it's expected to exceed the crystal surface energy values in the range $100-500 \times 10^3$, $2C$ is the crack length and E is the young's modulus.

3.9 Fatigue in graphite

Under cyclic stresses below the failure could occur, polycrystalline graphite shows fatigue failure, Green performed a test at 1950°C and it showed that the endurance limit of National Carbon Grade AUF increased with temperature and that limit was 17 MN/m² at low temperature and 30MN/m² at higher temperature, that when the number of cycles N>10⁴. Barabanov studied an anisotropic graphite in rotating bend parallel and perpendicular and got fatigue limits of 14MN/m² and 10MN/m², then Sato et al studied four separate graphites at ambient temperature in three stress modes; rotating bends, tension-compression and tension for N>10⁵ the fatigue limit for each case was 0.7-0.8 of the first cycle strength .

An alternative way of measuring material fatigue is to assume that most of the specimen fatigue life is depending on crack growth not the crack initiation as crack initiation is not necessary in polycrystalline graphite because of its high crack density, Marshall and Priddle both measured the crack growth rate in two nuclear graphites using a precracked tensile specimen and the results are

$$\frac{da}{dN} = C(\Delta K - \Delta K_0)^4 \quad (3.38)$$

where a is the crack length, ΔK is the applied range of stress intensity factor. C and ΔK_0 are constants , the prediction of the results were matching with the direct fatigue data, but when using this relation it indicates an arbitrary fatigue situation that doesn't produce crack growth. Brocklehurst took the stress intensity range

$$\Delta K = \Delta\sigma\sqrt{\pi a} \quad (3.39)$$

where $\Delta\sigma$ is the stress amplitude, to derive a relationship between the homologous stress σ/σ_l and $N\sigma_l^2$ for given ratios of $\Delta\sigma/\sigma$ and final crack length when failure occurs is given by:

$$K_c = \sigma\sqrt{\pi a_f} \quad (3.40)$$

The difference in crack length a with N is very rapid near failure that's why it is very difficult to detect the cracks growth before failure, there are some damages due to compressive stress cycles and they are 20% as damaging as the tensile cycles, for similar crack growth rates, higher strength material gives lower endurance than weak ones.

Green and Strahl have done two fatigue tests on extruded polycrystalline AUF graphite specimen at room temperature in terms of nominal fiber stress and number of cycles till failure, the tensile strength of graphite increases with increasing the temperature and the data in the following figure 27 shows that the endurance limit is about 4400 lb/in² at 3550°F with an increase of 75% over its room temperature and also the increasing of Brittleness which lead to elimination of the curve inclind. It is also shown that the increasing of the temperature increase the failure possibility on the first half-cycle of any stress greater than the endurance limit. In figure 28 it shows a specimen of brittle properties as it's broken without and fatigue crack propagation noticed at 3550, the fatigue behavior in AUF graphite is parallel to the extrusion axis at room temperature and also when the temperature was 3550 which indicates that graphite is suitable for alternating stresses conditions.^[12]

The difference between the specimens cut parallel and perpendicular to extrusion can be explained by the fact that during extrusion the anisometric grist tends to be aligned in the direction of extrusion, Losty discovered that permanent stress can be recovered by annealing at 1000°C and Jenkins discovered a way of recovery by neutron irradiation.^[12]

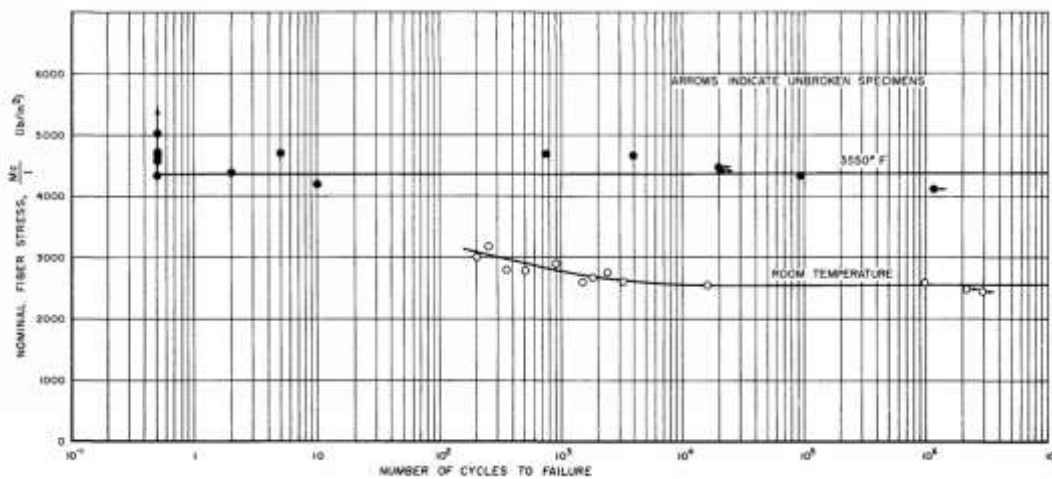


Figure 27

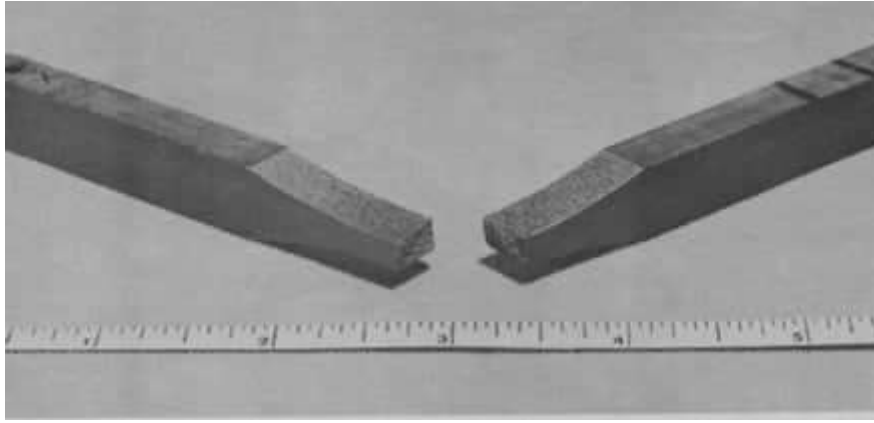


Figure 28 Typical specimen broken at 3550

3.10 Friction in graphite.^[13]

Graphite crystals have a very good cleavage parallel to the basal plane, and its low hardness in polycrystalline graphite makes it with high mechanicability properties on the contrary the less well graphitized carbons are found to be very difficult in machines with high hardness and poor lubricating action and machining process in such carbons cause breaking of primary valence bonds and the hardness is high.

The lubrication properties of the graphite causes the formation of surface coating of carbon hexagon networks on the slipping solids, graphite coatings have a high melting point and the formation of carbon networks ensures the absence of primary valence bonds that must be broken when certain movements happen to the graphite, and the movements of the layers lead to defects movements , figure 29 shows the relative movements of lamellae of graphite (plate 4)because of screw dislocations in the graphite

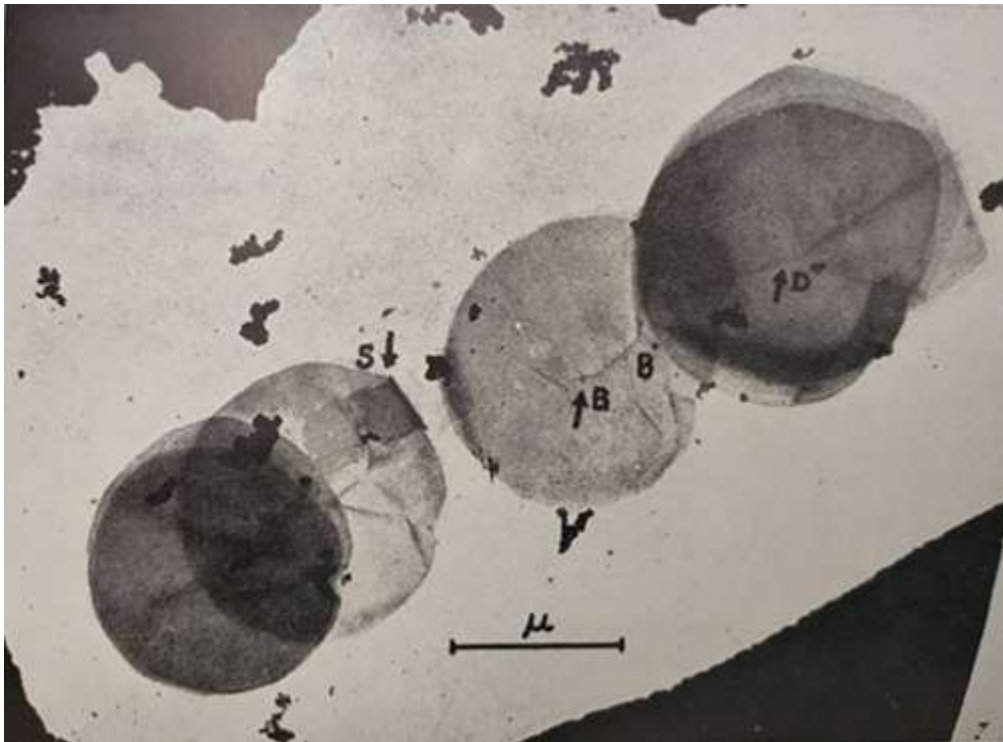


Figure 29 (a) Relative movement of lamellae of graphite sliding friction

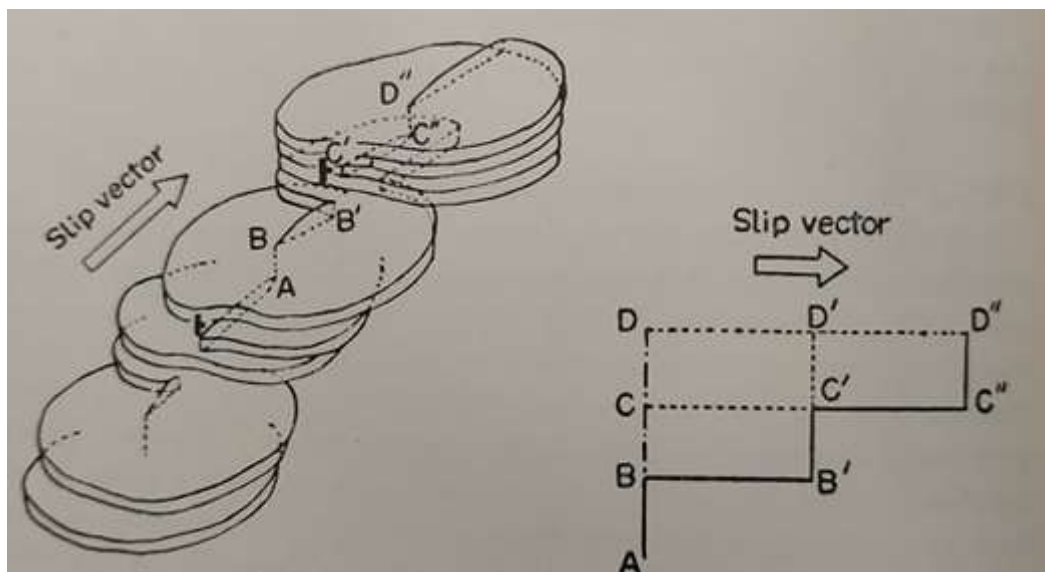


Figure 29 (b)

It is known that by strong heating in very high vacuum the surface films of the graphite could be removed because of the increasing of the frictional shearing forces between two surfaces and the increase of the friction coefficient is from 0.15 to about 0.5. However, we can reduce the friction coefficient to 0.3 by access this treated graphite to oxygen and water. It was noticed that heating in vacuum leads to permanent loss of peripheral impurity atoms and other defects whose their contribution gives a low friction coefficient of ordinary graphite. The adsorbed gases also can have other consequences on some applications of the

graphite, for example addition of small proportion of hydrocarbons of high molecular weight reduces the friction so for an aircraft designed to fly at high altitudes it is a problem.

The effect of adsorbed impurities on the frictional properties as in diamond the friction coefficient is about 0.5, when clean diamond surfaces are rubbed to each other, the surface became darker and as temperature is raised. Although this darkening happens below 1000°C, the film formed is stated to be identical with graphite in chemical and physical properties.

5. Conclusion

In conclusion this thesis collected an extensive recognition which was performed on the literature concerning the graphite properties, around twenty references and papers are included, and nearly twenty scientists experiments were explained with their results in order to obtain this bibliography about graphite structure and its properties.

6. References

- [1] N.B. Brandt, S.M. Chudinov, Y.G., Graphite and its compounds, North holland physics publishing, pages (2-11), (1988).
- [2] Keeler, James; Wothers, Peter, Chemical Structure and Reactivity, Oxford: OUP Oxford. Pages. 27–46. (1st ed.) (May 2008).
- [3] B.T, Kelly, Physics of graphite, Applied Science publishers, pages(34-120), (1981).
- [4] Web page, The Structure and Properties of Engineering Materials course, (archived in November 2001)
- [5] Spencer, Leonard James Crystallography Encyclopædia Britannica ,11th ed, pages 569–591,(1911).
- [6] Web Page, Encyclopedia.com High Beam Encyclopedia: aromatic compound, 2016
- [7] Ratner, Buddy D., Biomaterials science: an introduction to materials in medicine, 2nded., (2004).
- [8] J. R. Hahn, H. Kang ,Vacancy and interstitial defects at graphite surfaces: Scanning tunneling microscopic study of the structure, electronic property, and yield for ion-induced defect creation , Pohang university of science and technology, South Korea, (9 April 1999).
- [9] Helmut Sitter, Marian A. Herman, and W. Richter, Physical Principles and Technical Implementation, Springer,(2004).
- [10] L. Li,S. Reich,and J. Robertson, Defect energies of graphite: Density-functional calculations, University of Cambridge, (30 November 2005).
- [11] G.M.Jenkins, Analysis of the stress-strain relationships in reactor grade graphite, Berkeley Nuclear Laboratories, (1th September 1961).
- [12] L.Green, H.Strahl , The behavior of graphite under alternating stress, Atomic Energy Research Department, North American Aviation, INC, California, (4 May 1951).

- [13] A.R.Ubbelohde , F.R.S.,F.A.Lewis,Graphite and its crystal compounds, Oxford University press, pages(17-45), (1960).
- [14] Julie Chapman, Testing of Small Graphite Samples for nuclear qualifications, Idaho National Laboratory, USA, (November 2010).
- [15] U.Ramamurty, Mechanical Testing Methods of Fibers and Composites, Indian Institute of Science, Bangalore, India, (1 January 2003).
- [16] Carlotta Accettura, Ultra-high vacuum characterization of advanced materials for future particle accelerators, Master's thesis in Nuclear Engineering, Politecnico di Milano, 2016/2017
- [17] D.D.L. Chung, Carbon Fiber Composites,Butterworth-Heinemann.
- [18] A.Bertarelli, Novel materials for collimators at LHC nad its upgrads.
- [19] R. S. Lakes, "Foam structures with a negative Poisson's ratio", *Science* , 235 1038-1040, 1987
- [20] J. Gliick, The New York Times, 14 April 1987.
- [21] G. Milton, "Composite materials with Poisson's ratios close to -1", *J. Mech. Phys. Solids*, 40, 1105-1137, 1992
- [22] B. D. Caddock, and K. E. Evans, "Microporous materials with negative Poisson's ratio: I. Microstructure and mechanical properties", *J. Phys. D., Appl. Phys.* , 22, 1877-1882, **1989**.